

# JGR Atmospheres

## RESEARCH ARTICLE

10.1029/2021JD035705

### Key Points:

- Low ablation-season temperature caused low melt and a high proportion of snowfall, and led to glacier anomaly during 2000–2019 in the western Kunlun Mountains (WKM)
- Guliya experienced increased mass balance from 1970–1999 to 2000–2019 due to increased ablation-season precipitation related to changed Silk Road Pattern
- Warming caused the decreased mass balance of Guliya during 2000–2019 and will lead to future glacier mass loss in the WKM

### Supporting Information:

Supporting Information may be found in the online version of this article.

### Correspondence to:

H. Zhao and L. G. Thompson,  
zhaohb@ipcacs.ac.cn;  
thompson.3@osu.edu

### Citation:

Zhu, M., Yao, T., Yang, W., Wu, G., Li, S., Zhao, H., & Thompson, L. G. (2022). Possible causes of anomalous glacier mass balance in the western Kunlun Mountains. *Journal of Geophysical Research: Atmospheres*, 127, e2021JD035705. <https://doi.org/10.1029/2021JD035705>

Received 26 AUG 2021

Accepted 20 MAR 2022

### Author Contributions:

**Investigation:** Meilin Zhu, Guanjian Wu, Shenghai Li, Huabiao Zhao

**Methodology:** Wei Yang

**Project Administration:** Tandong Yao





**Resources:** Tandong Yao

**Writing – original draft:** Meilin Zhu,

Wei Yang, Huabiao Zhao

**Writing – review & editing:** Meilin Zhu, Lonnie G. Thompson

## Possible Causes of Anomalous Glacier Mass Balance in the Western Kunlun Mountains

Meilin Zhu<sup>1,2,3</sup> , Tandong Yao<sup>2</sup>, Wei Yang<sup>2</sup>, Guanjian Wu<sup>2</sup> , Shenghai Li<sup>2</sup> , Huabiao Zhao<sup>2,4</sup> , and Lonnie G. Thompson<sup>3</sup> 

<sup>1</sup>Center for the Pan-Third Pole Environment, Lanzhou University, Lanzhou, China, <sup>2</sup>State Key Laboratory of Tibetan Plateau Earth System, Resources and Environment (TPESRE), Institute of Tibetan Plateau Research, Chinese Academy of Sciences, Beijing, China, <sup>3</sup>Byrd Polar and Climate Research Center, The Ohio State University, Columbus, OH, USA, <sup>4</sup>Ngari Station for Desert Environment Observation and Research, Institute of Tibetan Plateau Research, Chinese Academy of Sciences, Beijing, China

**Abstract** Under current global warming, most glaciers on the Tibetan Plateau have shown significant mass loss during 2000–2019. However, the average glacier mass balance in the western Kunlun Mountains (WKM) was positive during this period. The causes of these opposing average status and the temporal glacier mass changes over the last several decades in the WKM continue to be the subject of active debate. The long-term mass balance of the Guliya Ice Cap (Guliya) in the WKM during 1970–2019 was reconstructed using an energy and mass balance model and calibrated ERA5 data, which was calibrated and validated by in situ measurements and geodetic mass balances. Guliya showed a positive mean mass balance during 2000–2019 because annual snowfall was larger than low ablation-season meltwater caused by low air temperature ( $T_a$ ). At interannual scales, annual mass balances were equally controlled by ablation-season precipitation and  $T_a$  during 1970–2019. From 1970s–1990s to 1990s–2010s, most Tibetan glaciers showed decreased mass balance due to increased ablation season  $T_a$ , while the WKM glaciers experienced increased mass balance due to increased ablation-season precipitation related to changes in the Silk Road Pattern. However, during 2000–2019, the annual mass balance of Guliya followed a decreasing trend due to increasing ablation-season  $T_a$ . The positive mass balance of the WKM glaciers will cease under future warming due to annual snowfall decreasing below ablation-season meltwater. These changes will threaten lives and livelihoods in the Tarim Basin, whilst also jeopardizing ice core-derived climate histories from the WKM glaciers.

## 1. Introduction

Glaciers in the Karakorum, eastern Pamir, and the western Kunlun Mountains (WKM) showed slightly positive mean mass balance and anomalous stability from 2000 to the 2010s, while most Tibetan glaciers underwent significant mass loss and widespread shrinkage (Brun et al., 2017; Shean et al., 2020; Yao et al., 2012; Ye et al., 2017; Zhou et al., 2018; Zhu et al., 2018b, Zhu, Yang, et al., 2021). These regional differences are known as the Karakoram Anomaly (Farinotti et al., 2020; Hewitt, 2005). Corresponding to this contrasting spatial pattern of glacier mass balance, long-term trends in ice flow velocities of most Tibetan Plateau (TP) glaciers showed a sustained slowdown, while glaciers of the Karakoram and WKM experienced slightly accelerated glacier flow during 2000–2017 (Dehecq et al., 2019). Another distinguishing characteristic of the Karakoram Anomaly is that frequent glacier surges occurred in the Karakoram and WKM over the last two decades, while glacier surging was largely absent for most regions of the TP (Farinotti et al., 2020). Evidence related to the Karakoram Anomaly is increasing with the greater availability of in situ measurements and satellite data.

Considering the importance of glaciers for regional water supplies and the cultural and religious value attributed to glaciers (Farinotti et al., 2020), several causes have been proposed to explain the anomalous behavior in the Karakoram, eastern Pamir, and the WKM. First, the Karakoram Anomaly could be associated with changes in climate forcing, which cause increased snowfall accumulation and/or reduced melting of snow and ice. Examples of this include the slowdown in warming since 2000 in the northwestern TP (Y. Wang et al., 2018), summertime cooling during 1979–2010 in the northwestern TP (Forsythe et al., 2017), and an increase in summer and/or winter snowfall and precipitation in the Karakoram, eastern Pamir, and the WKM (de Kok et al., 2020; Hewitt, 2005; Zhu et al., 2018b). Second, the Karakoram Anomaly could be related to changes in atmospheric circulation and land use, such as changes in Karakoram Vortex (Forsythe et al., 2017), mid-latitude climate (Zhu et al., 2018b),

and evapotranspiration from irrigation agriculture (de Kok et al., 2020). These variables can cause changes in the climatic factors described above. Third, the anomaly may be linked to these special glaciers and their regional climate and environmental conditions, such as winter precipitation in the Karakoram (Kapnick et al., 2014), the different area and thickness of glacier surficial debris cover (Scherler et al., 2011), regional differences in glacier mass balance sensitivity to climate change (de Kok et al., 2020; Sakai & Fujita, 2017; R. Wang et al., 2019; Zhu et al., 2018a), or regional differences in glacier distribution with altitude (Hewitt, 2005; Zhu et al., 2018b) and climatic conditions (Zhu et al., 2018a). Although these explanations have been proposed, understanding the full causes of the Karakoram Anomaly is far from complete due to differences in regional climate and the lack of direct glacio-meteorological observations that support model calibration and validation (Farinotti et al., 2020). This lack of data limits the potential for quantitative analysis to identify the climatic conditions that could lead to glacier growth.

Changes in climate variables can be used to explain the variability of glacier mass balance (Yang et al., 2016; Zhu et al., 2020; Zhu, Thompson, et al., 2021). For example, increased ablation-season precipitation has led to slight mass gains for the Muztag Ata No.15 Glacier in eastern Pamir over the last several decades (Zhu et al., 2018b). Some studies have shown that the Karakoram Anomaly in some regions of the Karakoram, eastern Pamir, and the WKM also occurred from the 1970s to 1999 (Y. Wang et al., 2018; Zhou et al., 2018) and may have begun in the 1940s (H. Zhao et al., 2021). These findings imply that the Karakoram Anomaly could be defined as the different mean or overall conditions of glacier mass changes for several decades between the WKM/eastern Pamir-Karakoram and most other regions of the TP and surrounding areas. As an important region with anomalous glacier behavior, glaciers in the WKM are excellent natural archives of paleo-climatic information (Pang et al., 2020; Thompson et al., 2018; Yao et al., 1997) and provide critical water resources for rivers in the Tarim Basin (Immerzeel et al., 2019). Comparing mean conditions during 2000–2010s for glaciers in the WKM with published values from representative glaciers in other regions of the TP can increase our understanding of the anomalous glacier average status in the WKM.

In addition to the average mass balance status over those periods, the temporal variability of glacier mass balance is also important to understand the relationship between climate drivers and glacier mass changes (Yang et al., 2016; Zhu, Thompson, et al., 2021). Quantifying this temporal variability can help us to explore the influence of glacier change on both water supplies and glacier-related hazards (Immerzeel et al., 2019; Yao et al., 2019) and predict future glacier evolution (Farinotti et al., 2020). However, recent information about the temporal variability of glacier mass balance over the last several decades in the WKM appears contradictory. For example, de Kok et al. (2020) found that the modeled glacier mass balance showed a decreasing trend for the WKM and Karakoram during 1980–2010, while remote sensing data showed that the average glacier mass balance over the WKM was slightly higher during 2000–2010s than during 1970s–2000 (Cao et al., 2020; G. Zhang et al., 2020). In addition, G. Zhang et al. (2020) indicated that region-wide glacier mass balance increased in the western part of the WKM but decreased in the eastern part, from 1970s–2000 to 2000–2018. Uncertainties in satellite data, different research regions, and the extent and timing of glacial surging can lead to differences in glacier mass balance measurements (Cao et al., 2020; G. Zhang et al., 2020).

To date, few studies have quantitatively investigated glacier mass change in the WKM and the response to climatic drivers due to the lack of in situ measurements of meteorological data and glacier mass balance. Glacier mass balance models and calibrated ERA5 data have been used to reconstruct long-term mass balance in the Himalayas (Azam & Srivastava, 2020; Sunako et al., 2019). Guliya is a typical WKM glacier (Figure 1; Li et al., 2019; Guo et al., 2015), with a slightly positive average mass balance from 2000 to the 2010s (Kutuzov et al., 2018; Lin et al., 2017). There is no evidence of surging during the period between 1970 and 2018 for Guliya (Cao et al., 2020), although one glacier, north of Guliya, surged (with no previous surging history) during July and early November 2015 (Muhammad & Tian, 2020). A glacier with no surging in the study period is better to understand the influence of climate on glacier mass change. Systematic glaciological and meteorological observations on Guliya from October 2015 to September 2019 are used to calibrate the ERA5 data. These data are used to drive the energy and mass balance (EMB) model that reconstructs the long-term mass balance of Guliya from 1970 to 2019. The aims of this study are: (a) to document the climate conditions driving the anomalous glacier mass balance from 2000 to the 2010s in the WKM, (b) to quantify the changes in mass balance from 1970 to 2019, and (c) to relate major drivers and thus establish the relationships between mass changes and atmospheric circulation in the WKM.

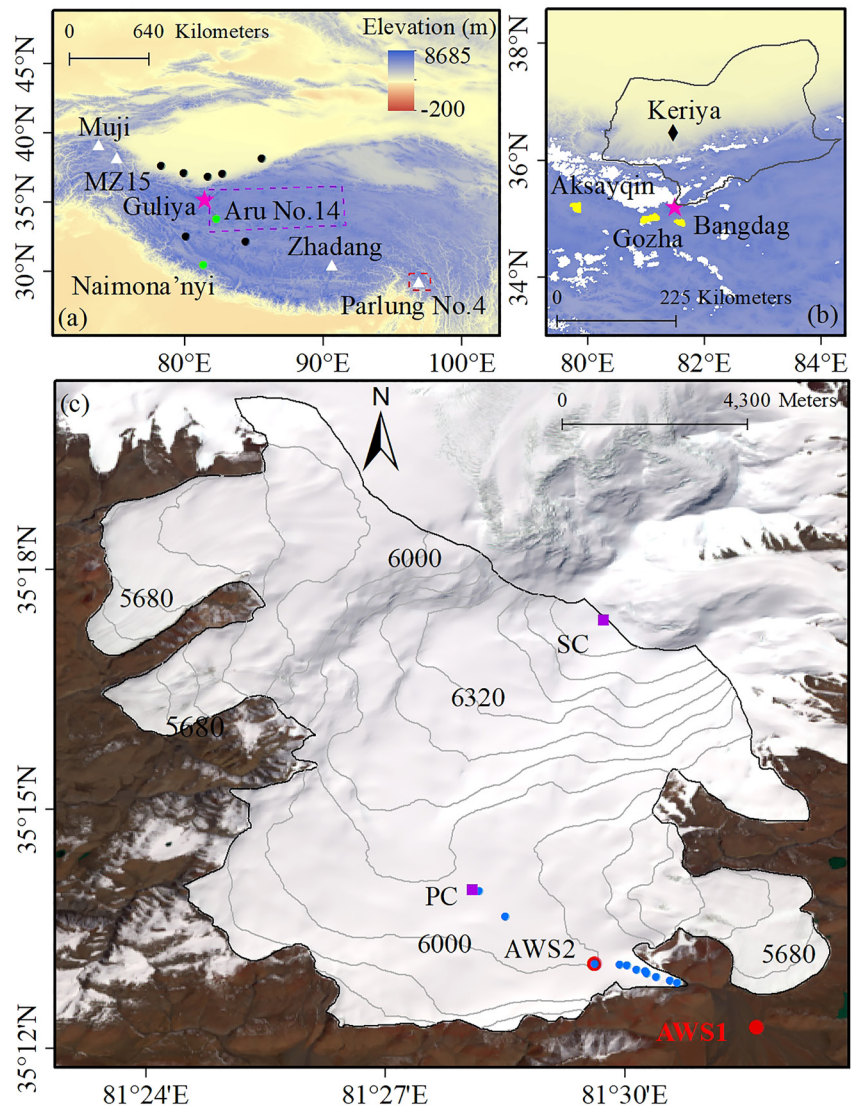


**Figure 1.** (a) Locations of Guliya (pink star) in the western Kunlun Mountains (WKM). The white triangles indicate the location of four other glaciers on the Tibetan Plateau. Black dots are the meteorological stations around the WKM and the two green dots mark the locations of the air temperature probes on Naimona'nyi and Aru No.14 glaciers. The purple and red dashed polygons indicate the northern Qiangtang Plateau and Kangri Karpo Mountains, respectively. (b) Locations of the Keriya Hydrological Station (black diamond), Guliya (pink star), Aksayqin, Nangdag, and Gozha Lakes (yellow shading), and the Keriya River basin (black line) are shown. Glaciers are marked by white colors. (c) Topographic map of the Guliya Ice Cap (80 m contours), showing the distribution of stakes (blue dots) installed in October 2018, the sites of AWS1 and AWS2 (red circles), and the sites of plateau ice core (PC, purple square) and summit ice core (SC, purple square) drilled on Guliya in October 2015.

## 2. Study Area, Data and Methods

### 2.1. Study Area

Guliya (81.4616°E and 35.2615°N) is a continental glacier (Shi & Liu, 2000) located on the southern slopes of the WKM (Figure 1a). This glacier provides meltwater to Gozha Co, which then flows into Lake Aksayqin. Guliya is also adjacent to the upper reaches of the Keriya River (Figure 1b). Under current climate conditions, the glacier is located within and near the southern boundary of the westerlies-dominated regime (Thompson et al., 2018; Yao et al., 2013). Guliya has an area of 111.4 km<sup>2</sup> and the elevation ranges from 5,487 to 6,650 m a.s.l. according to

the second Chinese glacier inventory (Guo et al., 2015). Most of the glacier surface is flat with an average slope of  $<3\text{--}5^\circ$ . The slope increases toward the summit and the east, where the outlet glaciers are located.

## 2.2. Data

Two automatic weather stations (AWS1 and AWS2) were installed on and near the southern edge of the ice cap in 2015 (Figure 1c). AWS2 was set up on the glacier surface at an elevation of 6,004 m a.s.l. and records the meteorological variables every half hour. These variables include wind direction (WD), wind speed (WS), air pressure (Press), air temperature ( $T_a$ ), relative humidity (RH), incoming and reflected solar radiation ( $S_{in}$  and  $S_{out}$ ), incoming and outgoing longwave radiation ( $L_{in}$  and  $L_{out}$ ), and distance from the sensor to glacier surface. AWS1 was set up on a small hill (5,491 m a.s.l.), approximately 1.6 km from the glacier terminus (Figure 1c). Half-hourly values of WD, WS, Press,  $T_a$ , RH,  $S_{in}$ , and precipitation ( $P_r$ ) were recorded. The sensors in the two AWSs and their specifications are provided in Table 1 of Li et al. (2019). The mass balance for Guliya was measured using the glaciological method (Cuffey & Paterson, 2010). Seven stakes were inserted into the glacier ice between 5,685 and 6,004 m a.s.l. in September 2015. The number of ablation stakes then progressively increased after September 2015 (Figure 1). Surface measurements were made at each stake at the beginning of October each year. These measurements included the stake reading and corresponding snow pit observations, such as snow depth and density measurements for each snow layer (Zhu, Yang, et al., 2021). We then derived the annual point mass balance at each stake. Point mass balance at the middle altitude at each individual interval was calculated by the interpolation and extrapolation of the point mass balance at the stakes. Using the area-averaged method described in Section 2.2.1 of Zhu, Yang, et al. (2021), the measured annual glacier-wide mass balance was calculated using the area for each interval, point mass balance at the middle altitude at each individual interval, and the total glacier area. Five temperature sensors with solar radiation shields were mounted on metal stakes at different altitudes near the ablation stakes. A mass balance year is defined as 1 October to 30 September of the next year.

To investigate glacier mass changes from a regional perspective, the following data products are utilized in the present investigation: (a) monthly and daily gridded data from the European Centre for Medium-Range Weather Forecasts (ERA5) ( $0.25^\circ \times 0.25^\circ$ , Hoffmann et al., 2019); (b) the standard monthly precipitation data from the CPC Merged Analysis of Precipitation (CMAP,  $2.5^\circ \times 2.5^\circ$ , Xie & Arkin, 1997); and (c) monthly gridded data from the Japanese 55-year reanalysis data set (JRA55,  $1.25^\circ \times 1.25^\circ$ , 1958–2019, Kobayashi et al., 2015). In addition, following Yasui and Watanabe (2010), the Silk Road Pattern (SRP) index is defined as the principal component of the leading mode for the 200 hPa meridional wind (V200) anomalies from JRA55, obtained through an empirical orthogonal function analysis in the domain  $20^\circ\text{--}60^\circ\text{N}$  and  $0^\circ\text{--}150^\circ\text{E}$ .

## 2.3. Energy and Mass Balance Model

To understand the interdecadal changes in mass balance on Guliya, we reconstructed the mass balance history during 1970–2019 at daily time intervals and at 40 m altitude intervals using the EMB model and calibrated ERA5 data. The EMB model used in this study is based on the point EMB model developed by Fujita and Ageta (2000). Here, we mainly present the most important features of the model. The model solves the following equation:

$$MB = \int \left( C_{en} + P_{snow} + \frac{Q_M}{L_m} + \frac{H_{lat}}{L_v} \right) dt \quad (1)$$

where point mass balance (MB) is composed of surface melt (or meltwater), sublimation/evaporation, refreezing ( $C_{en}$ ) and solid precipitation ( $P_{snow}$ ). Meltwater means the absolute value of the melt.  $Q_M$  is the melt energy.  $L_m$  is the latent heat of ice melt.  $H_{lat}$  is the latent heat flux.  $L_v$  is the latent heat of evaporation/sublimation.  $Q_M$  is calculated using the surface energy balance equation:

$$Q_M = S_{in}(1 - \alpha) + L_{in} + L_{out} + H_{sen} + H_{lat} + G \quad (2)$$

where  $\alpha$  is the albedo.  $H_{sen}$  is the sensible heat flux.  $G$  is the conductive heat flux. Net shortwave and longwave radiation are written as  $S_{net}$  and  $L_{net}$ , respectively.  $R_{net}$  is the sum of  $S_{net}$  and  $L_{net}$ .  $Q_M$  is defined as positive when it is larger than 0, and other fluxes are defined as positive when they are directed toward the surface. Here, we



used the model of Zhu, Thompson, et al. (2021), with a few modifications based on published work: albedo is calculated using the methods of Fujita and Sakai (2014).

The model inputs included the reconstructed long-term daily mean for  $T_a$ , RH,  $S_{in}$ , WS, and total daily precipitation, as well as their gradients and the glacier area in each elevation band. ERA5 data from the grid point (35°N and 78°75'E) around AWS2 were used to obtain meteorological forcing data from 1 October 1959 to 30 September 2019. The meteorological data (especially for annual precipitation) in that grid has the best relationship with the measured values from two AWSs. Time series of daily mean  $T_a$ , WS, RH, and  $S_{in}$  were constructed using a linear regression that was established between the ERA5 data and the available AWS2 data for each month, following similar methods to previous work (Zhu, Yang, et al., 2021). The reconstructed data and the observed meteorological variables are compared in Figure S1 of Supporting Information S1. The precipitation was reconstructed using the following two steps. First, the under-catch of precipitation was corrected based on temperature and WS during precipitation events (Q. Zhao et al., 2014). Daily precipitation was then reconstructed by applying a scaling factor of 1.16 to the total daily precipitation amount. The data were set as 0 when ERA5 daily precipitation in the corresponding grid was less than 0.45 mm, which is similar to Yang et al. (2013) and Zhu, Yang, et al. (2021). The cumulative precipitation amount, monthly precipitation and annual precipitation were used to assess the reliability of the reconstructed precipitation time series (Figure S2 in Supporting Information S1). These reconstructed meteorological data are referred to as calibrated ERA5 data in this work. The reconstructed and measured meteorological data are well correlated on different time scales, and the reconstructed meteorological data are reliable to drive the EMB model in this work.

The gradients of  $T_a$  and RH for the ablation season and the cold season (October–May) were based on data from five Hobo MX2301 sensors on the glacier from October 2018 to September 2020.  $P_r$  at different altitudes was estimated from AWS1 using three constant precipitation gradients ( $\Delta P_1$ ,  $\Delta P_2$ , and  $\Delta P_3$ ). The daily mean WS was assumed to be independent of altitude because the WS data on the glacier was considered too sparse to derive a general scheme to quantitatively assess the spatial distribution of WS (Hock & Holmgren, 2005). The daily mean  $S_{in}$  was assumed to be independent of altitude. Ice temperature at a depth of  $-10$  m was set to  $-11.6^\circ\text{C}$ , as measured in an ice borehole about 2.5 km away from AWS2 (Thompson et al., 2018). Previous studies have shown that the density of snowfall is between 50 and 169  $\text{kg m}^{-3}$  (Ding et al., 2017; Li et al., 2019). In this work, the density of snowfall was set to 100  $\text{kg m}^{-3}$ , which is similar to the assumption for the continental Xiao Dongkemadi Glacier (Fujita & Ageta, 2000). In addition, when the density of snowfall is changed from 100 to 200  $\text{kg m}^{-3}$ , the average mass balance during 1970–2019 only changed by 4 mm w.e.  $\text{a}^{-1}$  (Table S2 in Supporting Information S2). The influence of the density of snowfall on modeled long-term mass balance is small for Guliya. We do not consider the changes in the ice-covered area (the retreat of the glacier) or surface elevations during the study period because Guliya was largely stable or slightly gaining in mass over the last several decades (Lin et al., 2017; Muhammad & Tian, 2020). The glacier area distribution at each elevation band was derived from the glacier boundaries of the Second Glacier Inventory Data Set of China (Guo et al., 2015) and the 90 m Shuttle Radar Topography Mission digital elevation model (DEM).

These data were used to drive the EMB model for each 40 m interval (which is similar to the elevation bands used to calculate glacier-wide mass balance from observed point mass balance at the stakes) over the altitudinal range of the glacier. Using the area-averaged method described by Zhu, Yang, et al. (2021), glacier-wide mass balance, energy balance and their components were calculated. In our work, most physical parameters used in the EMB model were taken from measurements or published data. Unknown parameters required by the EMB model included  $\Delta P_1$ ,  $\Delta P_2$ ,  $\Delta P_3$ , and the bulk coefficient for sensible and latent heat fluxes ( $C_S$  and  $C_L$ ), parameters in the albedo model, and air-temperature thresholds for rain ( $T_{rain}$ ) and snow ( $T_{snow}$ ). Li et al. (2019) obtained the values for  $T_{rain}$  and  $T_{snow}$  on Guliya.  $C_S$  and  $C_L$  are often set to 0.002 (Fujita & Ageta, 2000). Most parameters in the albedo model were obtained from Fujita and Sakai (2014). As such, only  $\Delta P_1$ ,  $\Delta P_2$ ,  $\Delta P_3$ , and fresh snow albedo were adjusted to achieve the best match between the modeled and in situ mass balance (including the annual glacier-wide mass balance and point mass balance). First,  $\Delta P_1$  and fresh snow albedo were adjusted to minimize the root mean square error between in situ measured and modeled albedo, surface temperature, and surface height at AWS2, and between in situ measured and modeled mass balance at stakes below 6,020 m a.s.l. The values of parameters for the EMB model are presented in Table S1 of Supporting Information S2.

However, the modeled mass balance above 6,020 m a.s.l. was lower than the measured values at the stakes using the calibrated  $\Delta P_1$ . An elevation 6,020 m a.s.l. is in the interval of 6,000–6,040 m a.s.l. where the AWS2

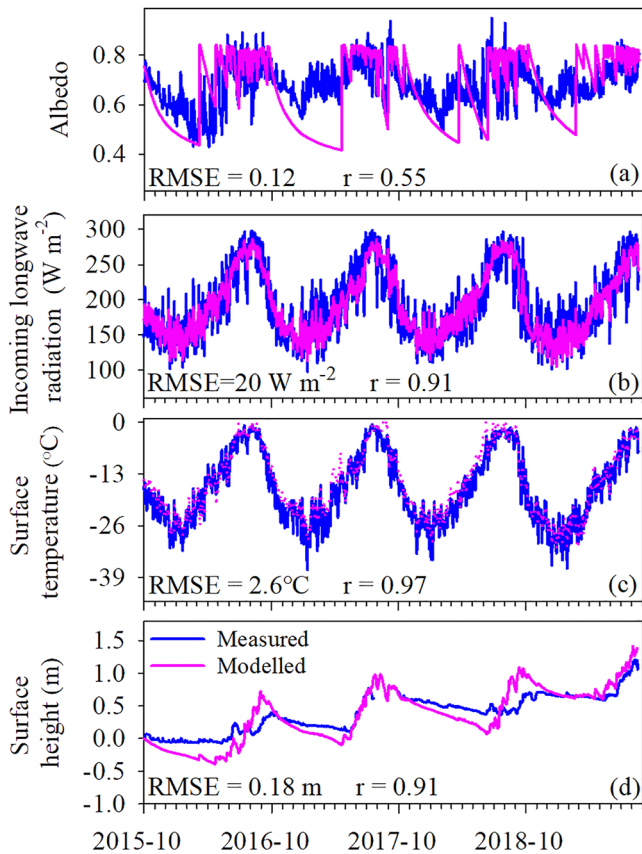


**Figure 2.** Comparisons of simulated results and observations at AWS2 on Guliya during the observation period: (a) daily mean albedo, (b) daily mean incoming longwave radiation, (c) daily mean surface temperature, and (d) glacier surface height. The  $L_{in}$  model is  $L_{in} = \sigma(T_a + 273.15)^4((1 - \tau_{atm}) + \tau_{atm} * (b_1 + b_2(\sqrt{e_a})))$ .  $\sigma$  is the Stefan–Boltzmann constant ( $5.67 \times 10^{-8} \text{ W m}^{-2} \text{ K}^{-4}$ ); Bulk atmospheric transmissivity ( $\tau_{atm}$ ) is the ratio of the measured incoming shortwave radiation to the incoming shortwave radiation at the top of the atmosphere;  $e_a$  is the vapor pressure (hPa). The two constants ( $b_1 = 0.4574$ ,  $b_2 = 0.1819$ ) were optimized using the measured  $L_{in}$ ,  $S_{in}$ , air temperature, relative humidity at AWS2. The modeled values are from the energy and mass balance model using reconstructed meteorological data from ERA5.

is located. We then used another precipitation gradient ( $\Delta P_2$ ) to model the mass balance between 6,020 and 6,600 m a.s.l. where the plateau core (PC) is located. We adjusted  $\Delta P_2$  to obtain the average mass balance at the site of the PC until a minimum difference between the in situ and modeled mass balance was achieved. The modeled depths were 6.6 and 5.7 m from 1993 to 2015 and from 1963 to 1992, respectively. These values are similar to the total length of the PC, which is 6.0 m from 1993 to 2015 and  $\sim 6.0$  m from 1963 to 1992 (Thompson et al., 2018). In addition, the modeled average mass balance during 2000–2015 at the PC site was  $357 \pm 121 \text{ mm w.e. a}^{-1}$ , which is similar to the geodetic average mass balance during 2000–2015 at the PC site ( $279 \pm 110 \text{ mm w.e. a}^{-1}$ ). The comparison of modeled point mass balance with point mass balance from the ice core and geodetic data at the drilling sites is reasonable over the last several decades, which is presented in Text S1 of Supporting Information S3.

There are flat areas above 6,600 m a.s.l., which is the summit of Guliya. Intense winter and spring winds may remove unconsolidated snow at the summit, which causes a much lower average annual layer thickness of the ice core at the summit than on the plateau (Thompson et al., 2018). We used the third precipitation gradient ( $\Delta P_3$ ) to model the mass balance above 6,600 m a.s.l. where the summit core (SC) is located. The  $\Delta P_3$  was adjusted to model the average mass balance at the SC site until a minimum difference between the in situ and modeled mass balance was achieved. The modeled average mass balance was 110 and 86 mm w.e. a<sup>-1</sup> during 1991–2015 and during 1963–1991, respectively. These two values are similar to the average mass balance from the SC, which was 112.5 mm w.e. a<sup>-1</sup> (125 ice equivalent a<sup>-1</sup>) from 1991 to 2015 and 62.1 mm w.e. a<sup>-1</sup> (69 ice equivalent a<sup>-1</sup>) during 1963–1992 (Thompson et al., 2018). In addition, the modeled average mass balance during 2000–2015 at the SC was 160 mm w.e. a<sup>-1</sup>, which is similar to the geodetic average mass balance during 2000–2015 at the PC site ( $270 \pm 110 \text{ mm w.e. a}^{-1}$ ). We modeled the long-term mass balance of Guliya from 1960 to 2019 to calibrate the EMB model using the average annual layer thickness of ice cores from Guliya. However, we mainly analyzed the long-term mass balance of Guliya during 1970–2019 because geodetic mass balance data can be obtained for this period (Lin et al., 2017; Zhou et al., 2018).

#### 2.4. Model Calibration, Validation and Uncertainty

The EMB model was calibrated and validated using 4-year in situ mass balance and meteorological data and the average annual layer thickness of ice cores from two sites on Guliya. Comparing the model results with field measurements was essential to evaluate the ability of the model to accurately capture surface EMB. Figure 2 shows that the observed albedo,  $L_{in}$ , surface temperature, and surface height at AWS2 agree well with the modeled values. Figure 3 compares the simulated and measured mass balance at stakes and for the whole glacier in different years. The good agreement between the simulated and measured mass balance validates the model's performance.

We also used the geodetic mean mass balance of regional glaciers in the WKM to validate the modeled mass balance of Guliya. According to the DEMs of different periods, the regional mean glacier mass balance in the eastern part of the western Kunlun region (containing Guliya) was  $60 \pm 160 \text{ mm w.e. a}^{-1}$  from the mid-1970s to 2000 (Zhou et al., 2018), and the mean mass balance of Guliya was  $230 \pm 55 \text{ mm w.e. a}^{-1}$  during 2000–2014 (Lin et al., 2017) and  $90 \pm 110 \text{ mm w.e. a}^{-1}$  during 2000–2015 (Kutuzov et al., 2018). These values are similar to the modeled average mass balance during 1974–1999 ( $4 \pm 121 \text{ mm w.e. a}^{-1}$ ), 2000–2014 ( $131 \pm 121 \text{ mm w.e. a}^{-1}$ ), and 2000–2015 ( $127 \pm 121 \text{ mm w.e. a}^{-1}$ ) in this work. Zhou et al. (2018) presented regionally averaged glacier mass balance in the eastern part of the WKM. Guliya is one of the largest glaciers in this region and accounts

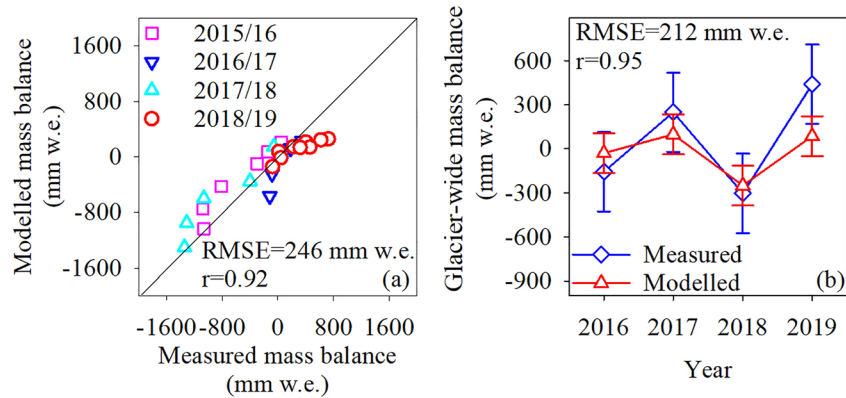


**Figure 3.** (a) Comparison between the modeled and measured mass balance at stakes and (b) comparison between the modeled and measured annual glacier-wide mass balance for different years with their uncertainties.

for 9.2% of the total glacier area (1208.8 km<sup>2</sup>, Zhou et al., 2018). The top of glaciers connects in this region, which means that these glaciers possibly experience similar changes. On decadal timescales, the large glaciers may have a similar average mass balance status (such as mass loss, main gain, or balanced conditions) to regional glaciers. For example, during the period 1973–2013, the mean annual mass balance for most single glaciers in Muztagh Ata was from  $-0.09 \pm 0.3$  to  $0.07 \pm 0.3$  m w.e. a<sup>-1</sup>, which is similar to the regionally averaged mass balance ( $-0.01 \pm 0.3$  m w.e. a<sup>-1</sup>) in this region (Holzer et al., 2015). In addition, during the period 2000–2014, the mean mass balance of Guliya was  $0.23$  m w.e. a<sup>-1</sup>, which was similar to the regionally averaged mass balance ( $0.174 \pm 0.058$  m w.e. a<sup>-1</sup>) of glaciers in the eastern part of the WKM (Lin et al., 2017). As such, the results from Zhou et al. (2018) can be used to qualitatively verify our modeled value of Guliya from the 1970s to 2000.

Guliya adjoins the upstream of the Keriya River, whose water is mainly derived from glacier meltwater from the eastern part of the WKM and precipitation in the Keriya River basin (Ma et al., 2019). Therefore, annual precipitation and glacier meltwater at Guliya are likely to be related to the runoff of the Keriya River. Figure 4 shows that the measured runoff depth at the Keriya Hydrological Station is correlated with annual precipitation on Guliya (without detrending,  $r = 0.57$ , and  $p < 0.01$ ; with detrending,  $r = 0.5$ , and  $p < 0.01$ ) and modeled ablation-season (June–September) glacier-wide meltwater for Guliya (without detrending,  $r = 0.5$ , and  $p < 0.01$ ; with detrending,  $r = 0.41$ , and  $p < 0.01$ ). The results confirm that the EMB model, driven by the calibrated ERA5 data, can satisfactorily reconstruct the long-term mass balance on Guliya.

The uncertainty in glaciological mass balance depends on uncertainties of in situ measurements of ablation and accumulation and on the extrapolation of point measurements to the entire glacier area. To estimate the uncertainties in point measurements of ablation and accumulation, we inserted two or three stakes in the same place (the distances between each stake was within 100 m) at several sites in the ablation and accumulation zone, respectively. The uncertainties in point measurements of ablation (130 mm w.e. a<sup>-1</sup>) and accumulation (100 mm w.e. a<sup>-1</sup>) were defined as the maximum standard deviation of the different stakes in the same place in the ablation zone and in the accumulation zone, respectively. Such differences contain the uncertainties in snow/firn density, snow thickness, and the rough surface at the interface between snow cover and ice at the stakes. The uncertainties in extrapolation for the ablation area ( $\pm 120$  mm w.e. a<sup>-1</sup>) and accumulation area ( $\pm 180$  mm w.e. a<sup>-1</sup>) were obtained from Kenzhebaev et al. (2017). Thus, the total uncertainty for measured annual glacier-wide mass balance was  $\pm 270$  mm w.e. a<sup>-1</sup> after adding all the parametric uncertainties using the error propagation law.

The uncertainties associated with the assumed values for unknown parameters (fresh snow albedo ( $a_{\text{fresh}}$ ), three precipitation gradients,  $T_{\text{snow}}$ ,  $T_{\text{rain}}$ ,  $C_S$ ,  $C_L$  and snowfall density) can greatly influence the model results. The uncertainty for  $a_{\text{fresh}}$  in the albedo model is unknown, and this parameter was changed by  $\pm 10\%$  from their original/calibrated values. The precipitation gradient was influenced by many factors, such as snowdrift and local topography, leading to a large uncertainty. In this work, uncertainties in  $\Delta P_1$ ,  $\Delta P_2$ , and  $\Delta P_3$  were defined as the standard deviation of these three values.  $T_{\text{snow}}$  was always set to 0°C (Zhu et al., 2018a) and the uncertainties for  $T_{\text{snow}}$  and  $T_{\text{rain}}$  were set to  $\pm 1.9^\circ\text{C}$ . The lower and upper bounds for  $C_S$  and  $C_L$  (0.0014 and 0.0026) were taken from

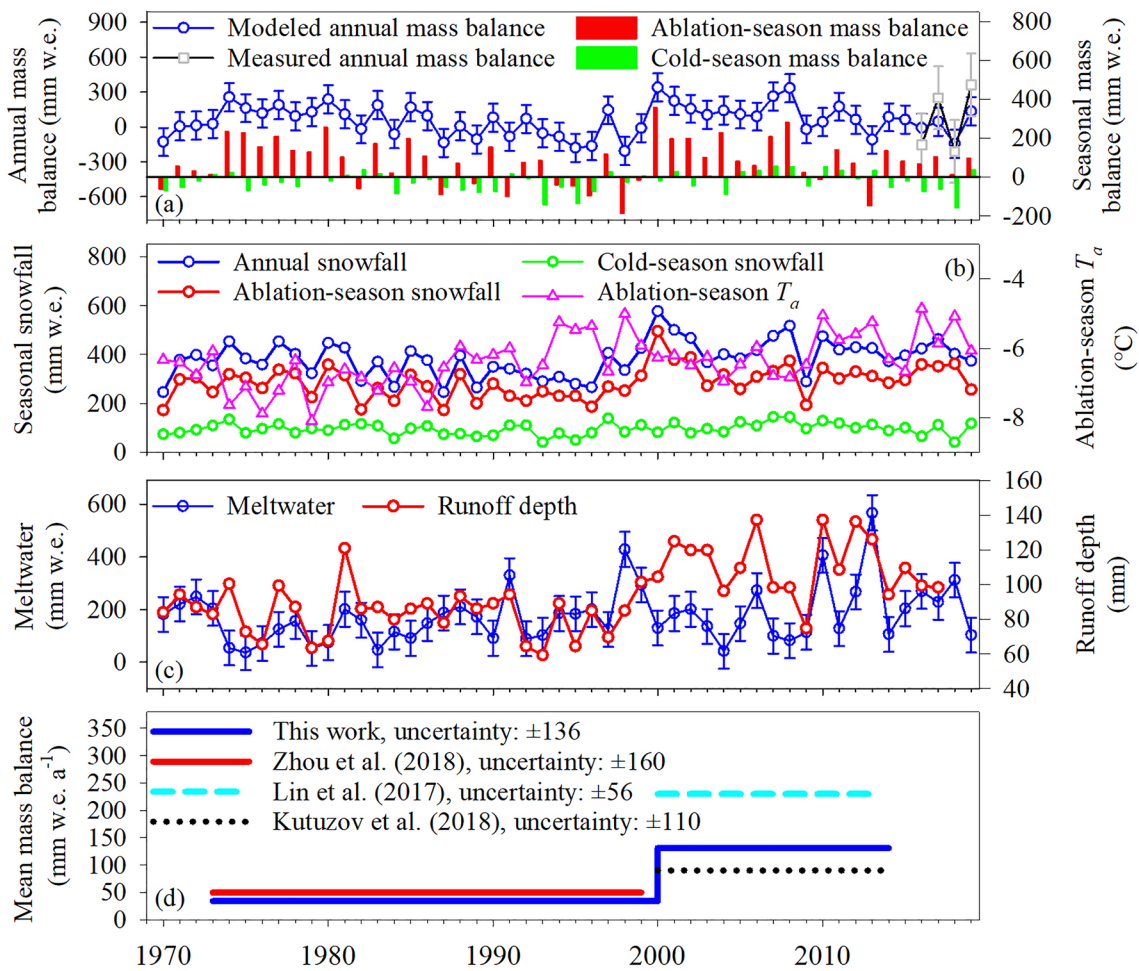


**Figure 4.** (a) The measured and modeled annual glacier-wide mass balances and modeled seasonal glacier-wide mass balances for Guliya; (b) seasonal glacier-wide snowfall on Guliya and ablation-season air temperature at AWS2 site; (c) modeled glacier-wide meltwater for Guliya in this work and measured runoff depth at Keriya Hydrological Station obtained from Ma et al. (2019); and (d) modeled and geodetic mean glacier-wide mass balance for different periods for Guliya, except for Zhou et al. (2018)'s result. Zhou et al. (2018)'s result is the regionally averaged glacier mass balance over the eastern part of the western Kunlun Mountains with glacier area of 1208.8 km<sup>2</sup> which contains Guliya. Meltwater indicates the absolute value of the melt. The year in the X axis indicates the balance year which is defined as 1 October to 30 September of the next year.

Li et al. (2019). We performed sensitivity tests to quantify the uncertainty in modeled annual mass balance by changing the assumed value for one input parameter at a time while leaving all other parameters unchanged. The parameter ranges used for the uncertainty estimation are given in Table S2 of Supporting Information S2. The total model uncertainty in annual mass balance was estimated by adding all the parametric uncertainties using the error propagation law (Azam & Srivastava, 2020; Zhu, Thompson, et al., 2021). The mean uncertainty for annual glacier-wide mass balance was estimated to be 121 mm w.e. a<sup>-1</sup> (Table S2 in Supporting Information S2). Using the method described above, the calculated mean uncertainty for annual glacier-wide meltwater was 66 mm w.e. a<sup>-1</sup> (Table S2 in Supporting Information S2).

Parameter sensitivity tests were conducted to find out which parameters significantly impact the modeled mass balance. Some previous studies have indicated that the modeled mass balance is more sensitive to parameters related to albedo because this can influence melt energy by changing available net shortwave radiation and glacier surface evolution (Li et al., 2019; Zhu et al., 2018b). Considering that  $a_{\text{fresh}}$  was changed by almost 0.1, we also changed the firn albedo ( $a_{\text{firn}}$ ) and ice albedo ( $a_{\text{ice}}$ ) by 0.1 to find out which parameters in the albedo model were more important to the modeled mass balance. We found that modeled mass balance was more sensitive to  $a_{\text{fresh}}$  and  $a_{\text{firn}}$  compared to  $a_{\text{ice}}$  (Table S2 in Supporting Information S2). This finding implies that the glacier surface was covered by snow for relatively long periods. In addition, sensitivities to precipitation gradients ( $\Delta P_1$  and



**Table 1**

Mean Seasonal Meteorological Variables at Stations and Glacier-Wide Mass Fluxes (mm w.e. a<sup>-1</sup>) on the Guliya Ice Cap in Different Periods for 1970–2019

Item	1970–2019			1970–1999			2000–2019			
	Cold	Ablation	Annual	Cold	Ablation	Annual	Cold	Ablation	Annual	
AWS2	$T_a$ (°C)	−21.3	−6.4	−14.5	−21.6	−6.6	−14.7	−20.9	−6.1	−14.2
AWS1	$P$ (mm)	74	221	295	70	201	271	79	251	330
Glacier-wide	Mass balance (mm w.e.)	−24	81	57	−33	60	27	−10	113	103
	Snowfall (mm w.e.)	96	287	383	91	261	352	103	325	428
	Refreezing (mm w.e.)	0	44	44	0	37	37	0	57	57
	Sublimation (mm w.e.)	−120	−75	−195	−124	−79	−203	−113	−70	−183
	Melt (mm w.e.)	0	−175	−175	0	−159	−159	0	−199	−199
	Precipitation (mm w.e.)	96	287	383	91	261	352	103	325	428

Note. Meltwater is the absolute value of melt.

$\Delta P_2$ ) were also very high on Guliya because the precipitation gradient directly influences snowfall accumulation and indirectly influences ablation. The low sensitivity to  $\Delta P_3$  (Table S2 in Supporting Information S2) is due to the small glacial area above 6,600 m a.s.l.  $C_S$  and  $C_L$  showed modest sensitivity because sublimation is also an important process that causes mass loss of Guliya.

### 3. Results and Discussion

#### 3.1. Temporal Changes in Mass Balance During 1970–2019

Guliya was in a balanced condition during 1970–2019, with a mean annual mass balance of  $57 \pm 121$  mm w.e. a<sup>-1</sup> (Table 1). The annual mass balance was positive in most years during 1970–1986, with a mean value of  $91 \pm 121$  mm w.e. a<sup>-1</sup>. The majority of annual mass balance values became negative during 1987–1999, with a mean value of  $-57 \pm 185$  mm w.e. a<sup>-1</sup> (Figure 4a and Table 1). These glacier mass changes contributed to a slightly positive mass balance during 1970–1999, which is coincident with the geodetic mean glacier mass balance in the eastern part of the WKM (Figure 4d), in the Gozha Co basin (G. Zhang et al., 2020), and on the southern slopes of the WKM (Cao et al., 2020). Although annual mass balance decreased during 2000–2019, the majority of annual mass balance values were positive from 2000 to 2019, with a mean value of  $102 \pm 121$  mm w.e. a<sup>-1</sup>. The positive mean mass balance during 2000–2010s for Guliya is also shown by the geodetic mean mass balance of Guliya (Figure 4d) and geodetic regional mean glacier mass balance in the WKM (Brun et al., 2017; Q. Wang et al., 2021).

In addition, we also analyzed the altitudinal profiles of modeled mean annual mass balance in different periods (Figure S3 in Supporting Information S1). Below ~5,960 m, glacier mass balance generally increased linearly with decreasing elevation. Between ~5,960 and ~6,560 m, glacier mass balance remained broadly steady with increasing elevation. Above ~6,560 m, glacier mass balance decreased with increasing elevation according to the snow layer thicknesses of two ice cores on Guliya (Thompson et al., 2018) and geodetic surface elevation change at those two drilling sites (Kutuzov et al., 2018). In addition, for the same altitudes below ~5,860 m (ablation zone), the mass balance was more negative during 2000–2019 than during 1970–1999 (Figure S3 in Supporting Information S1). This result is because the increased ablation-season  $T_a$  caused higher melt from 1970 to 1999 to 2000–2019 (Table 1). For the same altitudes in the accumulation zone, the mass balance was more positive during 2000–2019 than during 1970–1999 (Figure S3 in Supporting Information S1), mainly due to increased snowfall accumulation during 2000–2019 (Table 1).

The changes in annual mass balance mainly occurred in the ablation season by changing ablation-season snowfall and meltwater (Figure 4). Both ablation-season snowfall and meltwater showed the overall upward trends during 1970–2019 ( $p < 0.05$  via linear regression). The maximum value of ablation-season and annual snowfall during 1970–2019 occurred in 1999/2000 (Figure 4b), which had the largest annual layer thickness in the PC during

1970–2014 (Thompson et al., 2018). Ablation-season snowfall during 1970–1999 was always lower than that during 2000–2019 (Figure 4b). The modeled meltwater for Guliya showed low values and small interannual fluctuations from 1970 to 1998 and strong interannual fluctuations with increasing values from 1999 to 2019 (Figure 4c). The maximum ablation-season meltwater from 1970 to 2019 occurred in 2013/14.

Annual precipitation and ablation-season  $T_a$  can influence changes in mass balance by changing annual snowfall accumulation, ablation-season albedo, and thus ablation-season meltwater (Zhu et al., 2018a, Zhu, Yang, et al., 2021). Linear correlation analysis showed that annual mass balance displays strong relationships with annual precipitation (after detrending,  $r = 0.77$  and  $p < 0.01$ ), cold-season (October–May) precipitation (after detrending,  $r = 0.56$  and  $p < 0.01$ ), ablation-season precipitation (after detrending,  $r = 0.64$  and  $p < 0.01$ ) and ablation-season  $T_a$  (after detrending,  $r = -0.66$  and  $p < 0.01$ ). According to the sensitivity tests and variabilities of detrended ablation-season  $T_a$  ( $0.62^\circ\text{C}$ ), the detrended ablation-season precipitation (21.6%) and detrended cold-season precipitation (25.9%) during 1970–2019 (Zhu et al., 2020), changes in mass balance induced by ablation-season precipitation variability ( $89 \text{ mm w.e. a}^{-1}$ ) and the ablation-season  $T_a$  variability ( $92 \text{ mm w.e. a}^{-1}$ ) were similar and about two times larger than that induced by cold-season precipitation variability ( $44 \text{ mm w.e. a}^{-1}$ ). These results show that ablation-season precipitation and ablation-season  $T_a$  had almost an equal influence on changes in the annual mass balance of Guliya. Annual precipitation has a relatively larger influence on changes in the annual mass balance when compared to ablation-season  $T_a$ .

We further analyzed how ablation-season  $T_a$  and precipitation affected the changes in the annual mass balance. Ablation-season  $T_a$  can impact changes in the  $L_{\text{in}}$  and latent heat flux, which showed significant relationships with ablation-season melt energy (the  $r$  value between ablation-season  $L_{\text{in}}$  and melt energy and between ablation-season latent heat flux and melt energy is 0.67 and  $-0.41$ , respectively). The ablation-season melt energy, which is linked to the  $L_{\text{in}}$  and latent heat flux, can also impact the albedo and  $S_{\text{out}}$ . As such, the ablation-season  $T_a$  showed significant relationships with ablation-season albedo (after detrending,  $r = -0.52$  and  $p < 0.01$ ) and  $S_{\text{out}}$  (after detrending,  $r = -0.64$  and  $p < 0.01$ ). Through the above processes, ablation-season  $T_a$  can impact ablation-season meltwater (after detrending,  $r = 0.69$  and  $p < 0.01$ ), and thus annual mass balance.

In contrast, meltwater showed no significant relationship with ablation-season precipitation (after detrending,  $r = 0.05$  and  $p > 0.05$ ). Ablation-season precipitation showed a significant relationship with albedo (after detrending,  $r = 0.66$  and  $p < 0.01$ ) and  $S_{\text{out}}$  (after detrending,  $r = 0.45$  and  $p < 0.01$ ). These correlations are due to the fact that changes in ablation-season albedo and  $S_{\text{out}}$  related to changes in ablation-season precipitation have a small influence on changes in meltwater. The changes in albedo that are linked to changes in ablation-season precipitation can be assessed from the detrended ablation-season glacier-wide albedo minus the reconstructed albedo established by the linear relationship between the detrended ablation-season glacier-wide albedo and detrended ablation-season  $T_a$  at AWS2 (reconstructed albedo =  $-0.0247 \times T_a - 5\text{E-}16$ , determination coefficient ( $R^2$ ) = 0.29, and  $n = 50$ ). The above differences between these parameters showed no significant relationships with ablation-season meltwater ( $r = -0.15$  and  $p > 0.05$ ). Following a similar method, the changes in ablation-season  $S_{\text{out}}$  related to changes in ablation-season precipitation also exhibited no significant relationship with ablation-season meltwater ( $r = -0.16$ ,  $p > 0.05$ ). From the sensitivity tests and variabilities of detrended ablation-season  $T_a$  ( $0.62^\circ\text{C}$ ) and detrended ablation-season precipitation (21.6%) during 1970–2019 (Zhu et al., 2020), the change in meltwater induced by ablation-season precipitation variability ( $19 \text{ mm w.e. a}^{-1}$ ) was significantly smaller than that induced by the ablation-season  $T_a$  variability ( $97 \text{ mm w.e. a}^{-1}$ ). Therefore, for Guliya, ablation-season precipitation can influence changes in mass balance mainly by changing ablation-season snowfall accumulation, and ablation-season  $T_a$  can influence changes in the mass balance mainly by changing ablation-season meltwater.

### 3.2. Specific Climate Conditions That Were Conducive to Causing the Glacier Anomaly During 2000–2019 in the Western Kunlun Mountains

Modeled annual mass balance on Guliya was usually positive from 2000 to 2019 (Figure 4a), with a mean value of  $102 \pm 121 \text{ mm w.e. a}^{-1}$ . This finding was confirmed by the geodetic mean mass balance of Guliya (Figure 4d) and the geodetic regional mean glacier mass balance in the WKM (Brun et al., 2017; Q. Wang et al., 2021). The positive mean mass balance showed no direct relationship with the increased ablation-season (June–September)  $T_a$  and small changes in seasonal precipitation during this period (Figure 4). The dominant control on the mean

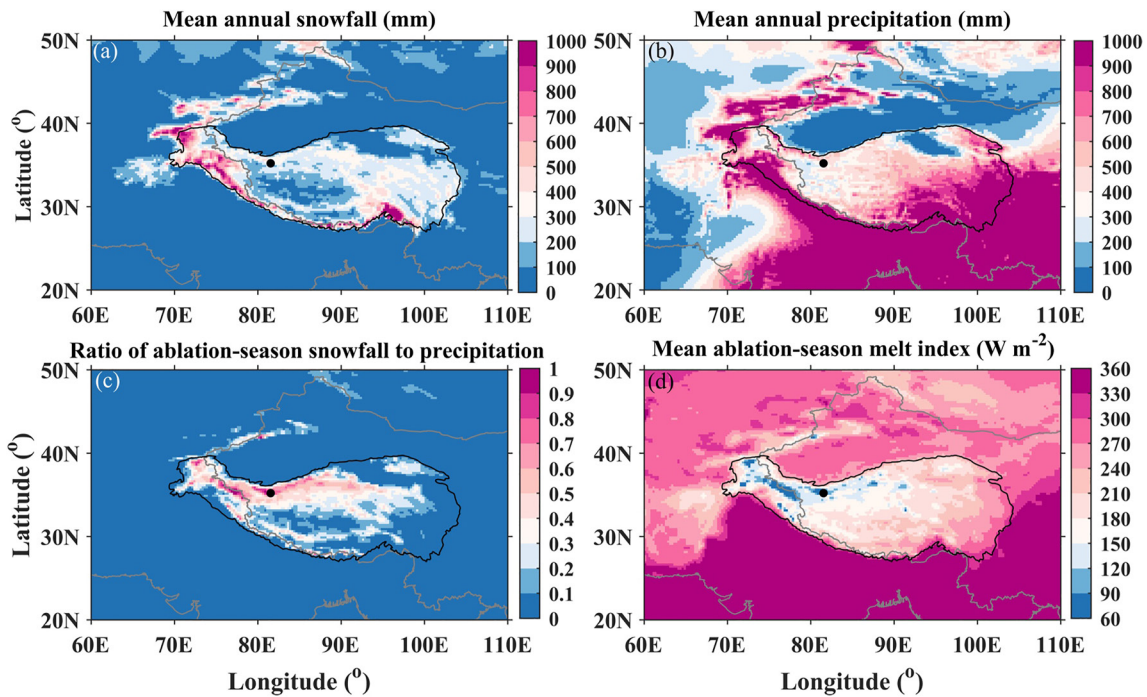


**Figure 5.** (a) The mean annual snowfall (mm), (b) mean annual precipitation (mm), (c) mean ratio of ablation-season snowfall to ablation-season precipitation (%), and (d) mean ablation-season melt index ( $W m^{-2}$ ) from 2000 to 2019. The melt index is defined as the sum of incoming longwave radiation (positive values) and outgoing shortwave radiation (negative values), according to Zhu et al. (2018a). The data is from the ERA5. The black dot indicates the location of Guliya.

annual mass balance was the differences between mean annual snowfall and mean ablation-season meltwater, which is related to the climate (Zhu et al., 2018a; Zhu, Yang, et al., 2021). The question is, what climatic factors drove the anomalously positive glacier mass balance in the WKM from 2000 to 2019 and how did they impact the two mass balance components?

**Table 2**

Mean Ablation-Season Glacier-Wide Temperature and Energy Fluxes on the Guliya Ice Cap in Different Periods for 1970–2019

Item	1970–2019	1970–1999	2000–2019	2000–2009	2010–2019
$T_s$ ( $^{\circ}C$ )	−6.1	−6.2	−5.9	−6.3	−5.5
$T_a$ ( $^{\circ}C$ )	−6.3	−6.5	−6.0	−6.4	−5.6
$S_{in}$ ( $W m^{-2}$ )	298	301	295	296	294
Albedo	0.76	0.75	0.76	0.77	0.75
$S_{out}$ ( $W m^{-2}$ )	−225	−225	−225	−229	−220
$S_{net}$ ( $W m^{-2}$ )	73	76	70	67	74
$L_{in}$ ( $W m^{-2}$ )	243	241	246	243	248
$L_{out}$ ( $W m^{-2}$ )	−289	−288	−290	−288	−292
$L_{net}$ ( $W m^{-2}$ )	−46	−47	−44	−45	−44
$H_{sen}$ ( $W m^{-2}$ )	−1	−1	0	0	0
$H_{lat}$ ( $W m^{-2}$ )	−19	−21	−18	−16	−21
$Q_G$ ( $W m^{-2}$ )	−2	−2	−2	−2	−1
$Q_m$ ( $W m^{-2}$ )	5	5	6	4	8

Note.  $T_s$  is the glacier-wide glacier surface temperature.

Ablation-season  $T_a$  and annual precipitation can impact snowfall accumulation and melt processes (Oerlemans, 2001; Zhu et al., 2018a; Zhu, Yang, et al., 2021). Mean annual precipitation during 2000–2019 was lower in the WKM than in most regions of the TP (Figure 5b), which contrasts the patterns of the mean glacier mass balance across the region. Thus, the assumption is that differences in mean ablation-season  $T_a$  contribute to these different mean glacier mass balance patterns. Compared to conditions on glaciers across most of the TP, lower  $T_a$  during 2000–2019 in the WKM resulted in lower  $L_{in}$  (Figure S4 in Supporting Information S1), lower turbulent heat fluxes (Table 2), and lower melt energy (Figure 5d), and also led to almost all of the precipitation falling as snow in the ablation season (Figure 5c and Table 1). Melt energy was smaller for the WKM glaciers compared to the majority of Tibetan glaciers (Figure 5d). For example, the average ablation-season melt energy on Guliya ( $6 W m^{-2}$ , Table 2) was significantly lower than on Zhadang ( $61 W m^{-2}$ ) and Parlung No. 4 glaciers ( $62 W m^{-2}$ ) in the southern TP (Zhu et al., 2018a), on Muji Glacier ( $21 W m^{-2}$ ) in the northeast Pamir (Zhu et al., 2020), and on Naimona'nyi Glacier ( $18 W m^{-2}$ ) in the western Himalayas (Zhu, Yang, et al., 2021). Although annual snowfall was moderate in the WKM when compared to other regions on the TP (Figure 5a), the mean annual snowfall was larger than the mean ablation-season meltwater at Guliya during 2000–2019 (Figure 4 and Table 1). This process led to higher mean albedo (Table 2) and a slightly positive average glacier mass balance

**Table 3**

Mean Seasonal Meteorological Variables at Automatic Weather Station Sties and Glacier-Wide Mass Fluxes (mm w.e.  $a^{-1}$ ) on the Guliya Ice Cap in Different Periods for 2000–2019

	Item	2000–2009			2010–2019		
		Cold	Ablation	Annual	Cold	Ablation	Annual
AWS2	$T_a$ ( $^{\circ}\text{C}$ )	−21	−6.4	−14.4	−20.7	−5.6	−13.9
AWS1	$P$ (mm)	83	255	338	76	246	322
Glacier-wide	Mass balance (mm w.e.)	0	172	172	−21	54	33
	Snowfall (mm w.e.)	107	331	438	98	319	417
	Refreezing (mm w.e.)	0	42	42	0	71	71
	Sublimation (mm w.e.)	−107	−61	−168	−119	−78	−197
	Melt (mm w.e.)	0	−140	−140	0	−258	−258

during 2000–2019, both for Guliya (Figure 4a) and for glaciers in the WKM in general (Cao et al., 2020; Lin et al., 2017).

For glaciers in most regions of the TP, the processes described above were reversed. The higher  $T_a$  led to larger  $L_m$  (Figure S4 in Supporting Information S1), turbulent heat fluxes, and thus higher melt energy for these glaciers when compared to WKM glaciers (Figure 5d). In addition, the high  $T_a$  also caused a substantial portion of precipitation to fall as rain on these glacier surfaces during the ablation season (Figure 5c) because the  $T_a$  was higher than the air temperature thresholds for snow (Zhu et al., 2018a). This increase in the proportion of precipitation falling as rain causes a reduction in ablation season and annual snowfall for most TP glaciers. Although annual precipitation is higher for glaciers in most regions of the TP than the WKM glaciers (Figure 5b), the differences in annual snowfall between the two regions are small (Figure 5a). This phenomenon is more significant in the ablation season (Figure S5 in Supporting Information S1). Under these conditions, ablation-season meltwater can be higher than annual snowfall for these glaciers, such as at Parlung No.4 Glacier (Zhu et al., 2018a) and glaciers in Hailuogou catchment (Y. Zhang et al., 2015) in southeastern TP, Zhadang Glacier (Zhu et al., 2018a) in the southern TP, glaciers in the central Himalayas (Bonekamp et al., 2019), Naimona'nyi Glacier on a north-facing slope in the western Himalayas (Zhu, Yang, et al., 2021) and Shiyi Glacier in the northeastern TP (H. Zhang et al., 2021). Overall, the mean mass balance for these glaciers outside the WKM was negative during 2000–2010s (Brun et al., 2017; Zhu, Yang, et al., 2021), accompanied by low ablation-season albedo (Zhu et al., 2018a).

Glacier-wide meltwater in the ablation season was lower on Guliya (Table 3) than that on Zhadang and Parlung No. 4 glaciers (Zhu et al., 2018a) during 2008–2013. These differences were because glacier-wide  $L_m$  was  $\sim 31 \text{ W m}^{-2}$  lower, the glacier-wide albedo was 0.18 higher, and glacier-wide turbulent heat flux (sum of sensible heat flux and latent heat flux) was  $\sim 19 \text{ W m}^{-2}$  lower on Guliya than Zhadang and Parlung No.4 glaciers. Ablation-season glacier-wide  $H_{\text{sen}}$  was close to 0 on Guliya because the difference between ablation-season glacier-wide glacier surface temperature ( $T_s$ ) and  $T_a$  was small (Table 2). Annual/ablation-season glacier-wide snowfall was 91/99 mm w.e.  $a^{-1}$  and 460/0 mm w.e.  $a^{-1}$  higher on Zhadang and Parlung No.4 glaciers (Zhu et al., 2018a) than on Guliya during 2008–2013. However, annual glacier-wide snowfall was 2.2 times higher than ablation-season glacier-wide meltwater, which resulted in a positive mean mass balance for Guliya during 2000–2019 (Figure 4 and Table 1). Ablation-season glacier-wide meltwater was significantly larger than annual glacier-wide snowfall, which resulted in a negative mean mass balance on Zhadang and Parlung No.4 glaciers during the 2000s–2010s (Zhu et al., 2018a).

Low  $T_a$  in the WKM may also be linked to factors other than high altitudes (Zhu et al., 2018b), such as the location (longitude, latitude), surrounding terrain, underlying surface, and regional atmospheric circulation. For these reasons, ablation-season  $T_a$  in 2018/19 measured at a similar altitude was significantly lower on Guliya ( $-6.3^{\circ}\text{C}$  at 6,004 m a.s.l.) than on Naimona'nyi Glacier ( $-2.7^{\circ}\text{C}$  at 5,980 m a.s.l.) and Aru No.14 Glacier ( $-4^{\circ}\text{C}$  at 6,013 m a.s.l.) (Figure 1a). As the  $L_m$ , turbulent heat fluxes and the ratio of snowfall to precipitation in the ablation season are linked to  $T_a$  (Zhu et al., 2018a), lower  $T_a$  may also cause lower mass sensitivity to precipitation ( $\pm 61 \text{ mm}$



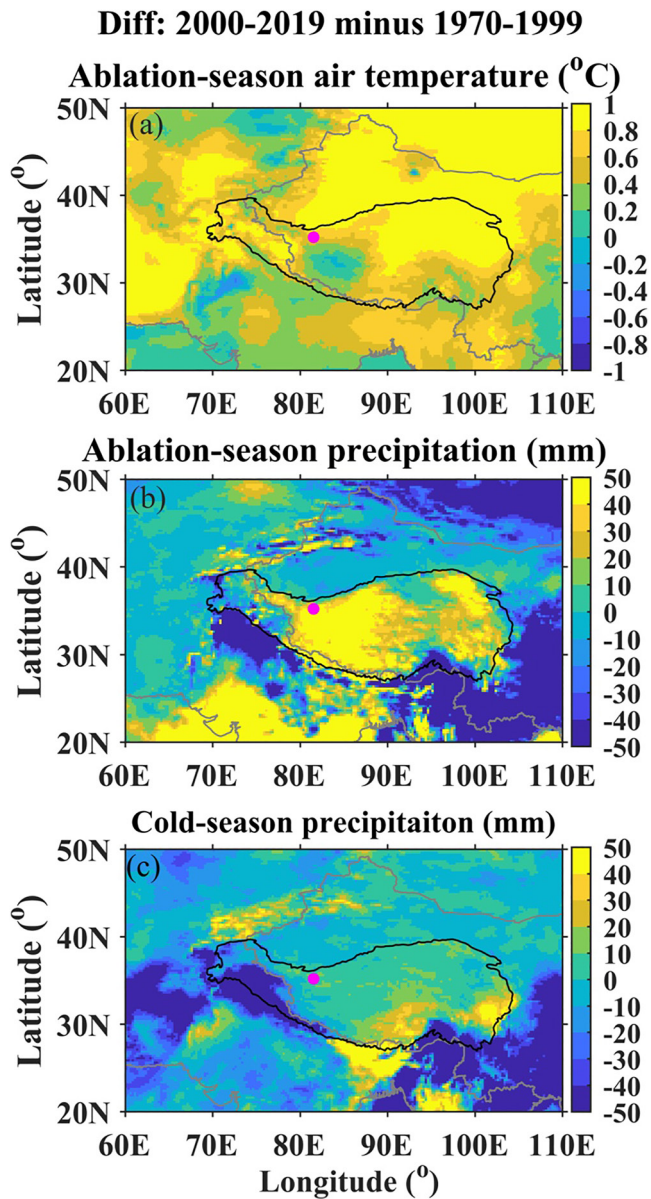


**Figure 6.** Differences in climate variables between the periods of 1970–1999 and 2000–2019: (a) ablation-season air temperature, (b) ablation-season precipitation, and (c) cold-season precipitation. The data is from ERA5. The pink dot indicates the location of Guliya. Difference: 2000–2019 minus 1970–1999.

w.e. (10%)<sup>-1</sup>) and air temperature ( $\pm 178$  mm w.e. °C<sup>-1</sup>) on Guliya, when compared to most glaciers on the TP (e.g., Zhu et al., 2018a, Zhu, Yang, et al., 2021).

To summarize, the low  $T_a$  meant that almost all precipitation fell as snow (i.e., a high snowfall proportion) and led to low ablation-season meltwater for the WKM glaciers. These conditions mean that ablation-season meltwater was lower than annual snowfall, and the mean annual glacier mass balance during 2000–2019 was positive in the WKM. These factors in the WKM can also explain a slightly positive mean mass balance during 1970–1999 for Guliya (Figure 4a) and for most WKM glaciers. These findings contrast to most of the TP glaciers, which have high melt energy and a large proportion of precipitation falling as rain during the ablation season, due to high  $T_a$ . These conditions meant that ablation-season meltwater was larger than annual snowfall, which caused negative mean mass balance during 2000–2010s.

### 3.3. Potential Causes of Interdecadal Changes in the Mass Balance of Glaciers in the Western Kunlun Mountains

Most glaciers on the TP and the surrounding areas have experienced an accelerating trend of mass loss from the 1970s–1990s to the 1990s–2010s, especially on glaciers in eastern Tian Shan, Himalayas, Qilian Mountains, southern TP, and western Tibet (Azam & Srivastava, 2020; Maurer et al., 2019; Shean et al., 2020; WGMS, 2020; Yang et al., 2016; Yao et al., 2012; Zhou et al., 2018; Zhu, Thompson, et al., 2021). Higher ablation-season  $T_a$  (Figure 6) resulted in decreased snowfall (due to a higher proportion of precipitation falling as rain) and increased  $L_{in}$  and turbulent heat fluxes (Zhu et al., 2018a, Zhu, Thompson, et al., 2021), which contributed to lower albedo and higher melt energy during the 1990s–2010s compared to the 1970s–1990s. These processes caused higher meltwater and lower snow accumulation during the 1990s–2010s. An alternative explanation is that ablation-season meltwater increased from the 1970s–1990s to the 1990s–2010s and was larger than the change in annual snowfall between the two periods. Thus, the mean annual mass balance for most glaciers on the TP was more negative during the 1990s–2010s than during the 1970s–1990s. In addition, lower cold-season (October–May) or ablation-season precipitation can also result in reduced annual snowfall accumulation, lower ablation-season albedo, higher ablation-season melt energy, and lower annual mass balance (Zhu, Yang, et al., 2021). The regional glacier mass loss rate from the 1970s–1990s compared to the 1990s–2010s in Kangri Karpo Mountains (Figure 1a) in the southeast TP was larger than most regions of the TP (Brun et al., 2017; Maurer et al., 2019; Wu et al., 2018; Yang et al., 2016; Zhou et al., 2018). This change was because ablation-season precipitation and cold-season precipitation decreased, while ablation-season  $T_a$  increased from the 1970s–1990s to 1990s–2010s (Figure 6).

These patterns contrast with WKM glaciers, which showed a slight increase in mean annual mass balance between the 1970s–1990s and 1990s–2010s. The average annual mass balance on Guliya was 96 mm w.e. a<sup>-1</sup> higher during 2000–2019 than during 1970–1999 (Figure 4a and Table 1), which is in accordance with the geodetic mass balance for Guliya (Figure 4d). The higher mean mass balance during 2000–2019 than during 1970–1999 on Guliya mainly occurred between 1987–1999 and 2000–2009 (Figure 4a). Most annual mass balance values were negative during 1987–1999 (with a mean value of  $-57 \pm 185$  mm w.e. a<sup>-1</sup>), and the annual mass balance was always larger during 2000–2009 than in other years (Figure 4a). The annual layer thickness of the ice core drilled on the plateau of Guliya showed an increasing trend during 1970–2014 (Thompson et al., 2018). This

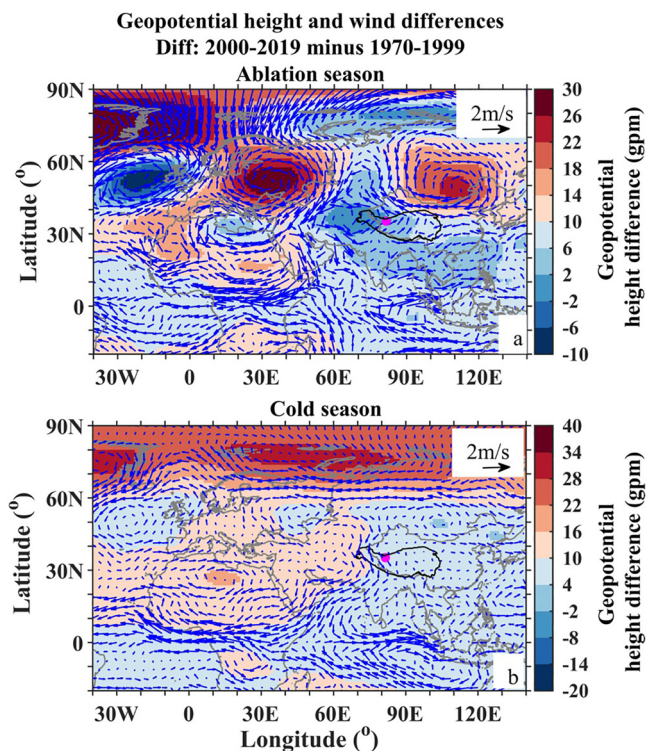


**Figure 7.** Differences in the mean 500 hPa geopotential heights (gpm) and wind speed (WS) fields ( $\text{m s}^{-1}$ ) between the periods of 1970–1999 and 2000–2019 during (a) the ablation season and (b) the cold season. The pink dot indicates the location of Guliya; the 500 hPa geopotential heights and WS fields were from the JRA55. Difference: 2000–2019 minus 1970–1999.

anomalies (Figure 7a) extended from the North Atlantic, across Europe, to the northeast of the eastern TP. The negative geopotential height anomalies and an anomalous cyclone appeared in the far western TP, while the positive geopotential height anomalies and anomalous cyclone appeared in the far northeastern TP (Figure 7a). Meanwhile, anomalous southerly winds occurred in the western TP. This circulation pattern is conducive to increased delivery of water vapor to the WKM through its southern regions, resulting in an increased net water vapor flux over the surrounding mountains (including the WKM) along the southern border of the Tarim Basin (C. Chen et al., 2020). Mölg et al. (2017) found that a similar cyclone in the far western TP and anticyclone in the high-latitudes of Europe can lead to anomalously high ablation-season precipitation in the WKM. The conditions shown in Figure 7a resemble the negative phase of the SRP on interdecadal scales (Figure 4b in Hong et al., 2017), suggesting that the SRP drove the changes in ablation-season precipitation between 1970–1999 and 2000–2019 in the WKM. When spatial correlations were performed using a 5-point Gaussian filter, negative correlations on interdecadal scales were found between the SRP index and ERA5/CMAP precipitation during the ablation season on the northern Qiangtang Plateau and in the WKM (Figure S7 in Supporting Information S1). However, the SRP can be influenced by many factors on interdecadal scales, such as the Atlantic Multidecadal Oscillation, sea surface temperatures in the northwestern Atlantic, and precipitation anomalies over the northeastern Indian continent (Liu et al., 2020; Han et al., 2021; Sun et al., 2020). These potential links require more investigation. During the cold season, the anticyclonic anomaly in the far western TP led to northerly wind anomalies over India and the western TP, which possibly reduced moisture transport to the WKM (Figure 7b). Cold-season precipitation changes between the two periods were insignificant in the WKM (Figure 6c). Studies have found that the cyclonic anomalies in the far western TP and southerly wind anomalies from the Arabian Sea and India to the western TP are conducive to the transport of moisture from the Arabian Sea to western TP adjacent to the WKM in winter (Qiu et al., 2019). In summary, most glaciers on the TP underwent accelerated mass loss from the 1970s–1990s to 1990s–2010s due to increasing ablation-season  $T_a$ , while the mean annual mass balance on Guliya was slightly

result also provides evidence for the increased mass balance on Guliya during this period, as the net accumulation of ice cores has been used as a proxy for precipitation change (H. Zhao et al., 2021) and mass balance variability (Duan et al., 2015). In addition, different types of remote sensing data show that the mean mass balance for WKM glaciers was slightly higher from 2000 to the 2010s than that from the 1970s to 2000 (Cao et al., 2020; G. Zhang et al., 2020).

The ERA5 data and meteorological stations around the WKM showed increasing ablation-season  $T_a$  and ablation-season precipitation and small changes in cold-season precipitation from 1970 to 1999 to 2000–2019 (Table S3 in Supporting Information S2 and Figure 6). The JRA55 data also showed similar patterns in ablation-season  $T_a$  and seasonal precipitation between the two periods (Figure S6 in Supporting Information S1). From 1970 to 1999 to 2000–2019, increasing  $T_a$  enhanced the meltwater during the ablation season on Guliya (Figure 4b) through increasing  $L_m$  and turbulent heat fluxes (Tables 2 and 3). The precipitation increased by  $50 \text{ mm a}^{-1}$  during the ablation season and by only  $9 \text{ mm a}^{-1}$  during the cold season, according to the calibrated precipitation at AWS1 (Table 1). The sensitivity analysis described in Text S2 of Supporting Information S3 shows that from 1970 to 1999 to 2000–2019 increased ablation-season precipitation in the form of snowfall was the primary contributor to the higher mass balance. This change compensated for the mass loss that was driven by the rising ablation-season  $T_a$ . In addition, increased snowfall accumulation may refreeze more meltwater in the snow cover, and this likely played a minor role in the higher mass balance during 2000–2019 than during 1970–1999.

To further support this view and to explore the influence of atmospheric circulation on mass changes in the WKM, we analyzed the differences in seasonal circulation patterns (500 hPa geopotential height and wind fields) between 1970–1999 and 2000–2019 (Figure 7). A zonal wave-like feature during the ablation season in the 500 hPa geopotential height and wind

higher during 2000–2019 than during 1970–1999, mainly due to increasing ablation-season precipitation, which may have been related to the changes in phases of the SRP.

### 3.4. The Possible Changes in Mass Balance for the Guliya Ice Cap During 2000–2019

The annual mass balance on Guliya decreased slightly during 2000–2019 (Figure 4a and Table 3), which is similar to the result from remote sensing data of the WKM (Hugonnet et al., 2021). Muhammad and Tian (2020) demonstrated that most of the ice thickening on Guliya during 2004–2015 occurred between 2004 and 2008. The glacier area on the southern slopes of the WKM increased from 2000 to 2010 and decreased from 2010 to 2018 (Cao et al., 2020). Thus, it is possible that the average mass balance during 2000–2009 was slightly higher than that during 2010–2019. Such changes were mainly caused by increasing ablation-season  $T_a$  during 2000–2019 (Text S3 in Supporting Information S3), which increased the  $L_m$  and turbulent heat fluxes and reduced albedo and enhanced melt energy (Table 3 and Table S4 in Supporting Information S2). Ablation-season and cold-season precipitation during 2010–2019 increased by 21% and 56%, respectively, which would have counteracted the increased mass loss during 2000–2019 caused by the increased ablation-season  $T_a$ . ERA5 data of cold-season and ablation-season precipitation showed only a slight change around the WKM between 2000–2009 and 2010–2019 (Zhu, Thompson, et al., 2021). This finding implies that the strength of seasonal precipitation variability was not significant enough to control the mass balance change between the two periods.

Although there are no direct long-term measurements of  $T_a$  in the WKM, indirect evidence indicates that ablation-season  $T_a$  increased during 2000–2019. Compared to low-altitude meteorological stations in the Tarim Basin, data from high-altitude meteorological stations such as Gaize and Shiquanhe show higher ablation-season  $T_a$  during 2010–2019 than during 2000–2009 (Table S3 in Supporting Information S2). Moderate Resolution Imaging Spectroradiometer (MODIS) daytime land surface temperature for summer during 2001–2015 increased throughout the WKM (Cai et al., 2017). Daily cloud-free MODIS snow cover products show that snow cover days in the Gozha Basin decreased in all seasons during 2003–2017 (G. Zhang et al., 2020). The increase in annual water level in Bangdag Co was  $\sim 2$  times higher during 2000–2009 than during 2010–2015 (Qiao et al., 2017). These changes were driven by a likely increase in ablation-season  $T_a$  in the WKM during 2000–2019 rather than by decreased annual precipitation. These findings suggest that ablation-season  $T_a$  in the WKM was increasing during 2000–2019.

The Indian summer monsoon (ISM) will likely intensify with future global warming (Roxy, 2017). The enhanced ISM may reduce moisture transport from the Indian Ocean to the WKM and the Tarim Basin (Y. Zhao et al., 2014). In turn, this change may reduce ablation-season precipitation on Guliya, indicated by the negative relationship between annual layer thickness in the Guliya ice core record and the ISM index on decadal time scales (Thompson et al., 2018). The increasing ablation-season  $T_a$  and reducing ablation-season precipitation will enhance melt energy and reduce snowfall accumulation on the WKM glaciers. When glacier meltwater is larger than the annual snowfall, WKM glaciers will change from mass gain to mass loss as the equilibrium line altitudes rise. As the glacier mass is reduced, the conditions on the glaciers will have a lower compacity to adjust the runoff of the rivers in the Tarim Basin. These glaciers are extremely important in providing meltwater during drought periods, preserving snowfall in times of flood, and are likely to lose more mass from higher elevations in the future. It is likely that the current period of positive balance of the WKM glaciers will end under continuous climate warming, which will pose potential threats to the lives and livelihoods in Tarim Basin and ice core-derived climate histories preserved by the WKM glaciers (Thompson et al., 2021).

### 3.5. The Influence of Changes in Glacier Area and Elevation on Modeled Mass Balance for the Guliya Ice Cap

According to the Chinese Glacier Inventory, there were 423 glaciers with a total area of 2965.35 km<sup>2</sup> in the 1970s in the WKM (Shi et al., 2008). The glaciers (changes in areas, lengths, and mass balances on decadal timescales) were relatively stable in the WKM (Brun et al., 2017; Lin et al., 2017; Y. Wang et al., 2018; Yao et al., 2012), where some surge-type glaciers have been found (Guan et al., 2022; Yasuda & Furuya, 2015). Glacier surging can modify the glacier area, surface velocity, and surface elevation. If surge-type glaciers increase the glacier area at low altitudes, glacier ablation will increase, leading to more mass loss. However, the initiation time and duration of the active phase of glacier surging varied greatly for different glaciers in the WKM (Guan et al., 2022). It is



difficult to estimate the influence of glaciers surging on changes in regional glacier mass balance on interdecadal timescales. Guan et al. (2022) found that glaciers in the WKM were divided into one of four categories: seven confirmed surge-type glaciers, one likely surge-type glacier, eight possible surge-type, and 407 non-surge-type glaciers. Therefore, most WKM glaciers were relatively stable without discernible surging.

The glacier area shrinkage rate in the WKM was  $3.6\% \pm 4.8\%$  or  $0.07\% \pm 0.1\% \text{ a}^{-1}$  during 1968–2017, which is not significant (Y. Wang et al., 2018). Glacier area changes in the WKM over the past 40 years are characterized by spatial and temporal heterogeneity (Y. Wang et al., 2018). The area of the glaciers on the south and north slopes of the WKM decreased significantly from 1972 to 1991 (Cao et al., 2020). From 1991 to 2010, the area of the north slope decreased, and the area of the south slope increased. From 2010 to 2018, the area of the north slope increased significantly, and the area of the south slope decreased (Cao et al., 2020). In addition, some large glaciers in this region showed complicated variations. For example, some glaciers presented short-term (one or several years) advances within a retreating trend during 1972–2020, while some exhibited a continuous advance or continuously retreated (Guan et al., 2022). However, most glaciers (about 405, including large and small glaciers and Guliya) in the WKM had a relatively stable terminus position, with total variations of  $<0.12 \text{ km}$  during 1972–2020 (Guan et al., 2022). Thus, our assumption that ice-covered areas on Guliya did not change during 1970–2019 is reasonable.

Glacier volume estimation is based on volume-area scaling ( $V = c \times A^\gamma$ , where  $V$  and  $A$  are the volume and area of a single glacier, respectively, and  $c$  and  $\gamma$  are scaling parameters; Bahr et al., 1997). Therefore, when the changes in glacier area are small, the glacier volume will be stable for Guliya and most WKM glaciers over the last several decades. This fact means that changes in regionally averaged mass balance over the last several decades were small, which is also verified by the geodetic mass balance data in the WKM. These data show that glaciers in the WKM were close to balanced conditions during 1970–1999, with a regionally averaged mass balance of  $-0.06 \pm 0.13 \text{ m w.e. a}^{-1}$  (Y. Wang et al., 2018) and  $0.02 \pm 0.1 \text{ m w.e. a}^{-1}$  (Zhou et al., 2018), and that glaciers in the WKM are slight positive during 2000–2010s, with the regionally averaged mass balance from  $0.04 \pm 0.15$  to  $0.16 \pm 0.1 \text{ m w.e. a}^{-1}$  (Brun et al., 2017; Shean et al., 2020; R. Wang et al., 2019). The regionally averaged mass balance of glaciers in the eastern part of the WKM and the average mass balance of Guliya also showed similar values for the two periods (Lin et al., 2017; Y. Wang et al., 2018; Zhou et al., 2018; Figure 4a).

The spatial-temporal patterns of glacier velocities in the WKM are complicated. The velocities in the center-line within the ablation zone of some glaciers were larger in summer ( $\sim 0.3 \text{ m d}^{-1}$ ) compared to those in winter ( $<0.05 \text{ m d}^{-1}$ ) during 2017–2019, while the velocities of some glaciers were faster during winter than during summer (Guan et al., 2022). For surge-type glaciers, Yasuda and Furuya (2015) found that the surface velocity is faster in early winter than in summer because of the presence of surface meltwater that reroutes through the englacial and subglacial drainage. On interannual timescales, some large glaciers in the WKM showed variable changes in surface velocities (acceleration, deceleration, and relative stability) in different periods during 1991–2020, although most glaciers in the WKM had slow velocities with little variation (Guan et al., 2022). For example, the modeled mean annual horizontal ice flow speeds of Guliya were relatively low (less than  $20 \text{ m/a}$ ), and the ice flow velocities on the terminus and the ablation zone were lower compared to those in the accumulation zone (W. Chen et al., 2017). Guliya also has a low velocity without apparent motion on most parts of the surface in winter (Yan et al., 2015). Guliya is the most stable glacier in China due to the relatively small changes in the strain rate and the low ice temperature near the glacier terminus (W. Chen et al., 2017).

Interannual fluctuations in the glacier-wide mass balance are mainly due to temperature and precipitation changing accumulation and ablation processes (Oerlemans, 2005). Our modeled surface mass balance results showed that the glacier surface is decreasing at low altitudes due to mass loss and is increasing at high altitudes due to mass accumulation. However, glacier movements can also move mass from high altitudes to low altitudes. These shifts mean that glacier thicknesses are reduced at high altitudes and increased at low altitudes. Theoretically, for a stationary glacier with zero mass balance, the glacier thicknesses (from the glacier surface to the bedrock) will show no change in both the ablation and accumulation zone (Tian et al., 2014). These mean changes in glacier elevations are small for non-surge-type glaciers in the WKM, according to their geodetic mass balance data. For example, the total changes in glacier height for non-surge-type glaciers in the WKM during 2000–2014 was from  $-5.8 \text{ m}$  at  $5,300 \text{ m a.s.l.}$  to  $3.7 \text{ m}$  at  $6,700 \text{ m a.s.l.}$  (Lin et al., 2017). The two cores at the same drill site on Guliya from different years provide further information to show that the changes in altitude of Guliya are small. The ice core to bedrock is  $309.73 \text{ m}$  in 2015, which is only  $1.13 \text{ m}$  longer than in 1992. Thus, the changes in glacier



surface height, resulting from the mass accumulation and ablation processes, are reduced by the glacier dynamic process. These processes caused small changes in the elevation or morphology of Guliya on interdecadal timescales, meaning that the influence of small changes in the surface elevation of Guliya on the modeled long-term mass balance will be small. As such, our assumption that the surface elevations on Guliya did not change during 1970–2019 is reasonable.

#### 4. Conclusion

The mass balance history of Guliya in the WKM from October 1969 to September 2019 was reconstructed using an EMB model and calibrated ERA5 data. The key objectives of this work were to analyze the average mass balance status during 2000–2019, quantify the temporal variability of the mass balance in different periods and explore the potential driving mechanisms. The model was calibrated and validated by annual layer thickness measurements obtained from two ice cores drilled on Guliya, in situ meteorological data at AWS2, the mass balance at different stakes, the geodetic mass balance data from Guliya and the majority of glaciers in the WKM, and the measured runoff depth at Keriya Hydrological Station. Guliya experienced overall mass gain during 2000–2019 because low  $T_a$  caused low ablation-season meltwater that was lower than annual snowfall. The low  $T_a$  in the WKM was linked to low  $L_{in}$  and turbulent heat fluxes and high ratios of snowfall to precipitation (a high snowfall proportion). In contrast, in most of the TP, high  $T_a$  caused high melt energy and a large proportion of precipitation falling as rain during the ablation season. These processes caused ablation-season meltwater to be larger than annual snowfall, and the majority of glaciers in this region experienced a negative mean mass balance during 2000–2010s. At interannual timescales, ablation-season precipitation and ablation-season  $T_a$  had a nearly equal influence on changes in the mass balance of Guliya. Ablation-season precipitation can influence changes in mass balance mainly by changing ablation-season snowfall accumulation, and ablation-season  $T_a$  can influence changes in the mass balance mainly by changing ablation-season meltwater. From the 1970s–1990s to 1990s–2010s, most glaciers on the TP and the surrounding areas showed increased mass loss due to increased ablation-season  $T_a$ , while the WKM glaciers showed an increase in the mean mass balance. The mean mass balance for Guliya was slightly higher during 2000–2019 than during 1970–1999 due to increasing ablation-season precipitation, which may be related to changes in the phase of the SRP. From 2000 to 2009 to 2010–2019, the mean mass balance of Guliya decreased due to increasing ablation-season  $T_a$ . Future global warming will result in that the status of the majority of glaciers will change from mass gain to mass loss when the annual snowfall becomes lower than ablation-season meltwater. This shift will pose potential threats to the lives and livelihoods of people in the Tarim Basin, and will jeopardize ice core-derived climate histories preserved in WKM glaciers. The drivers for changes in mass balance varied during different periods, due to different strengths of climate variability for these periods. This phenomenon has been found in Zhu, Thompson, et al. (2021). Overall, more observations of WKM glaciers are needed to fully understand the influence of climate drivers on glacier behavior.

#### Data Availability Statement

JRA-55 and ERA5 reanalysis data sets are freely distributed on the National Center for Atmospheric Research (<http://rda.ucar.edu/datasets/ds628.1/>) and the Climate Data Store (<https://cds.climate.copernicus.eu/cdsapp#!/search?type=dataset>), respectively. The CMAP precipitation data was provided by the NOAA/OAR/ESRL PSD (<https://www.esrl.noaa.gov/psd/>). The calibrated ERA5 data and reconstructed mass balance of Guliya Ice Cap are deposited in National Tibetan Plateau Data Center (<https://doi.org/10.11888/Cryos.tpcdc.272203>).

#### References

- Azam, M. F., & Srivastava, S. (2020). Mass balance and runoff modelling of partially debris-covered Dokriani Glacier in monsoon-dominated Himalaya using ERA5 data since 1979. *Journal of Hydrology*, 590, 125432. <https://doi.org/10.1016/j.jhydrol.2020.125432>
- Bahr, D. B., Meier, M. F., & Peckham, S. D. (1997). The physical basis of glacier volume-area scaling. *Journal of Geophysical Research*, 102, 20355–20362. <https://doi.org/10.1029/97JB01696>
- Bonekamp, P. N., de Kok, R. J., Collier, E., & Immerzeel, W. W. (2019). Contrasting meteorological drivers of the glacier mass balance between the Karakoram and central Himalaya. *Frontiers in Earth Science*, 7, 107. <https://doi.org/10.3389/feart.2019.00107>
- Brun, F., Berthier, E., Wagnon, P., Kääh, A., & Treichler, D. (2017). A spatially resolved estimate of High Mountain Asia glacier mass balances, 2000–2016. *Nature Geoscience*, 10(9), 668–673. <https://doi.org/10.1038/NGEO2999>
- Cai, D., You, Q., Fraedrich, K., & Guan, Y. (2017). Spatiotemporal temperature variability over the Tibetan Plateau: Altitudinal dependence associated with the global warming hiatus. *Journal of Climate*, 30(3), 969–984. <https://doi.org/10.1175/JCLI-D-16-0343.1>

#### Acknowledgments

The authors acknowledge the staff at the Ngari Station for Desert Environment Observation and Research, Institute of Tibetan Plateau Research, Chinese Academy of Sciences, for help in the field. This study is jointly funded by the Strategic Priority Research Program of Chinese Academy of Sciences (grant XDA2006020102), National Natural Science Foundation of China (Grants 41971092, 41771085, and 4191101270), the Second Tibetan Plateau Scientific Expedition and Research Program (2019QZKK0201), National Key Research and Development Project (2019YFC1509102), and National Science Foundation Paleo Perspectives on Climate Change (Award 1502919). We thank the anonymous reviewers for their constructive comments.

- Cao, B., Guan, W., Li, K., Wen, Z., Han, H., & Pan, B. (2020). Area and mass changes of glaciers in the West Kunlun Mountains based on the analysis of multi-temporal remote sensing images and DEMs from 1970 to 2018. *Remote Sensing*, *12*(16), 2632. <https://doi.org/10.3390/rs12162632>
- Chen, C., Zhang, X., Lu, H., Jin, L., Du, Y., & Chen, F. (2020). Increasing summer precipitation in arid Central Asia linked to the weakening of the East Asian summer monsoon in the recent decades. *International Journal of Climatology*, *41*, 1024–1038. <https://doi.org/10.1002/joc.6727>
- Chen, W., Liu, S., Li, W., Wang, W., & Wang, R. (2017). An analysis of the ice temperature and velocity along the main flowline of Guliya Ice Cap of Western Kunlun Mountains based on glacier dynamical model. *Chinese Science Bulletin*, *62*(33), 3910–3920. <https://doi.org/10.1360/N972017-00676>
- Cuffey, K., & Paterson, W. S. B. (2010). *The physics of glaciers* (4th ed., p. 693). Elsevier.
- Dehecq, A., Gourmelen, N., Gardner, A. S., Brun, F., Goldberg, D., Nienow, P. W., et al. (2019). Twenty-first century glacier slowdown driven by mass loss in High Mountain Asia. *Nature Geoscience*, *12*, 22–27. <https://doi.org/10.1038/s41561-018-0271-9>
- de Kok, R. J., Kraaijenbrink, P. D., Tuinenburg, O. A., Bonekamp, P. N., & Immerzeel, W. W. (2020). Towards understanding the pattern of glacier mass balances in High Mountain Asia using regional climatic modelling. *The Cryosphere*, *14*(9), 3215–3234. <https://doi.org/10.5194/tc-14-3215-2020>
- Ding, B., Yang, K., Yang, W., He, X., Chen, Y., LazhuGuo, X., et al. (2017). Development of a water and enthalpy budget-based glacier mass balance model (WEB-GM) and its preliminary validation. *Water Resources Research*, *53*(4), 3146–3178. <https://doi.org/10.1002/2016WR018865>
- Duan, K., Xu, B., & Wu, G. (2015). Snow accumulation variability at altitude of 7010 m asl in Muztagh Ata Mountain in Pamir Plateau during 1958–2002. *Journal of Hydrology*, *531*, 912–918. <https://doi.org/10.1016/j.jhydrol.2015.10.013>
- Farinotti, D., Immerzeel, W. W., de Kok, R. J., Quincey, D. J., & Dehecq, A. (2020). Manifestations and mechanisms of the Karakoram glacier Anomaly. *Nature Geoscience*, *13*, 8–16. <https://doi.org/10.1038/s41561-019-0513-5>
- Forsythe, N., Fowler, H. J., Li, X., Blenkinsop, S., & Pritchard, D. (2017). Karakoram temperature and glacial melt driven by regional atmospheric circulation variability. *Nature Climate Change*, *7*(9), 664–670. <https://doi.org/10.1038/nclimate3361>
- Fujita, K., & Ageta, Y. (2000). Effect of summer accumulation on glacier mass balance on the Tibetan Plateau revealed by mass-balance model. *Journal of Glaciology*, *46*(153), 244–252. <https://doi.org/10.3189/172756500781832945>
- Fujita, K., & Sakai, A. (2014). Modelling runoff from a Himalayan debris-covered glacier. *Hydrology and Earth System Sciences*, *18*(7), 2679–2694. <https://doi.org/10.5194/hess-18-2679-2014>
- Guan, W., Cao, B., Pan, B., Chen, R., Shi, M., Li, K., et al. (2022). Updated surge-type glacier inventory in the West Kunlun Mountains, Tibetan Plateau, and implications for glacier change. *Journal of Geophysical Research: Earth Surface*, *127*, e2021JF006369. <https://doi.org/10.1029/2021JF006369>
- Guo, W., Liu, S., Xu, J., Wu, L., Shangguan, D., Yao, X., et al. (2015). The second Chinese glacier inventory: Data, methods and results. *Journal of Glaciology*, *61*(226), 357–372. <https://doi.org/10.3189/2015JG014J209>
- Han, Y., Ma, W., Yang, Y., Ma, Y., Xie, Z., Sun, G., et al. (2021). Impacts of the Silk Road pattern on the interdecadal variations of the atmospheric heat source over the Tibetan Plateau. *Atmospheric Research*, *260*, 105696. <https://doi.org/10.1016/j.atmosres.2021.105696>
- Hewitt, K. (2005). The Karakoram Anomaly? Glacier expansion and the “elevation effect”, Karakoram Himalaya. *Mountain Research and Development*, *25*, 332–340. [https://doi.org/10.1659/0276-4741\(2005\)025\[0332:TKAGEA\]2.0.CO;2](https://doi.org/10.1659/0276-4741(2005)025[0332:TKAGEA]2.0.CO;2)
- Hock, R., & Holmgren, B. (2005). A distributed surface energy-balance model for complex topography and its application to Storgraciären, Sweden. *Journal of Glaciology*, *51*(172), 25–36. <https://doi.org/10.3189/172756505781829566>
- Hoffmann, L., Günther, G., Li, D., Stein, O., Wu, X., Griessbach, S., et al. (2019). From ERA-Interim to ERA5: The considerable impact of ECMWF's next-generation reanalysis on Lagrangian transport simulations. *Atmospheric Chemistry and Physics*, *19*(5), 3097–3124. <https://doi.org/10.5194/acp-19-3097-2019>
- Holzer, N., Vijay, S., Yao, T., Xu, B., Buchroithner, M., & Bolch, T. (2015). Four decades of glacier variations at Muztagh Ata (eastern Pamir): A multi-sensor study including Hexagon KH-9 and Pléiades data. *The Cryosphere*, *9*, 2071–2088. <https://doi.org/10.5194/tc-9-2071-2015>
- Hong, X. W., Lu, R. Y., & Li, S. L. (2017). Amplified summer warming in Europe–West Asia and Northeast Asia after the mid-1990s. *Environmental Research Letters*, *12*, 094007. <https://doi.org/10.1088/1748-9326/aa7909>
- Hugonnet, R., McNabb, R., Berthier, E., Menounos, B., Nuth, C., Girod, L., et al. (2021). Accelerated global glacier mass loss in the early twenty-first century. *Nature*, *592*(7856), 726–731. <https://doi.org/10.1038/s41586-021-03436-z>
- Immerzeel, W. W., Lutz, A. F., Andrade, M., Bahl, A., Biemans, H., Bolch, T., et al. (2019). Importance and vulnerability of the world's water towers. *Nature*, *577*, 364–369. <https://doi.org/10.1038/s41586-019-1822-y>
- Kapnick, S. B., Delworth, T. L., Ashfaq, M., Malyshev, S., & Milly, P. C. D. (2014). Snowfall less sensitive to warming in Karakoram than in Himalayas due to a unique seasonal cycle. *Nature Geoscience*, *7*, 834–840. <https://doi.org/10.1038/ngeo2269>
- Kenzhebaev, R., Barandun, M., Kronenberg, M., Chen, Y. N., Usabaliyev, R., & Hoelzle, M. (2017). Mass balance observations and reconstruction for Batysh Sook Glacier, Tien Shan, from 2004 to 2016. *Cold Regions Science and Technology*, *135*, 76–89. <https://doi.org/10.1016/j.coldregions.2016.12.007>
- Kobayashi, S., Ota, Y., Harada, Y., Ebata, A., Moriya, M., Onoda, H., et al. (2015). The JRA-55 reanalysis: General specifications and basic characteristics. *Journal of the Meteorological Society of Japan. Series II*, *93*(1), 5–48. <https://doi.org/10.2151/jmsj.2015-001>
- Kutuzov, S., Thompson, L. G., Lavrentiev, I., & Tian, L. (2018). Ice thickness measurements of Guliya ice cap, western Kunlun Mountains (Tibetan Plateau), China. *Journal of Glaciology*, *64*(248), 977–989. <https://doi.org/10.1017/jog.2018.91>
- Li, S., Yao, T., Yu, W., Yang, W., & Zhu, M. (2019). Energy and mass balance characteristics of the Guliya ice cap in the West Kunlun Mountains, Tibetan Plateau. *Cold Regions Science and Technology*, *159*, 71–85. <https://doi.org/10.1016/j.coldregions.2018.12.001>
- Lin, H., Li, G., Cuo, L., Hooper, A., & Ye, Q. (2017). A decreasing glacier mass balance gradient from the edge of the Upper Tarim Basin to the Karakoram during 2000–2014. *Scientific Reports*, *7*(1), 1–9. <https://doi.org/10.1038/s41598-017-07133-8>
- Liu, Y., Zhou, W., Qu, X., & Wu, R. G. (2020). An interdecadal change of the boreal summer Silk Road pattern around the late 1990s. *Journal of Climate*, *33*, 7083–7100. <https://doi.org/10.1175/jcli-d-19-0795.1>
- Ma, X., Yan, W., Zhao, C., & Kundzewicz, Z. W. (2019). Snow-cover area and runoff variation under climate change in the West Kunlun Mountains. *Water*, *11*(11), 2246. <https://doi.org/10.3390/w11112246>
- Maurer, J. M., Schaefer, J. M., Rupper, S., & Corley, A. (2019). Acceleration of ice loss across the Himalayas over the past 40 years. *Science Advances*, *5*(6), eaav7266. <https://doi.org/10.1126/sciadv.aav7266>
- Mölg, T., Maussion, F., Collier, E., Chiang, J. C. H., & Scherer, D. (2017). Prominent midlatitude circulation signature in high Asia's surface climate during monsoon. *Journal of Geophysical Research*, *122*, 12702–12712. <https://doi.org/10.1002/2017JD027414>
- Muhammad, S., & Tian, L. (2020). Mass balance and a glacier surge of Guliya ice cap in the western Kunlun Shan between 2005 and 2015. *Remote Sensing of Environment*, *244*, 111832. <https://doi.org/10.1016/j.rse.2020.111832>
- Oerlemans, J. (2001). *Glaciers and climate change*. AA Balkema Publishers.

- Oerlemans, J. (2005). Extracting a climate signal from 169 glacier records. *Science*, *308*, 675–677. <https://doi.org/10.1126/science.1107046>
- Pang, H., Hou, S., Zhang, W., Wu, S., Jenk, T. M., Schwikowski, M., & Jouzel, J. (2020). Temperature trends in the northwestern Tibetan Plateau constrained by ice core water isotopes over the past 7,000 years. *Journal of Geophysical Research*, *125*(19), e2020JD032560. <https://doi.org/10.1029/2020JD032560>
- Qiao, B., Zhu, L., Wang, J., Ju, J., Ma, Q., & Liu, C. (2017). Estimation of lakes water storage and their changes on the northwestern Tibetan Plateau based on bathymetric and Landsat data and driving force analyses. *Quaternary International*, *454*, 56–67. <https://doi.org/10.1016/j.quaint.2017.08.005>
- Qiu, T., Huang, W., Wright, J. S., Lin, Y., Lu, P., He, X., et al. (2019). Moisture sources for wintertime intense precipitation events over the three snowy subregions of the Tibetan Plateau. *Journal of Geophysical Research*, *124*(23), 12708–12725. <https://doi.org/10.1029/2019JD031110>
- Roxy, M. (2017). Land warming revives monsoon. *Nature Climate Change*, *7*, 549–550. <https://doi.org/10.1038/nclimate3356>
- Sakai, A., & Fujita, K. (2017). Contrasting glacier responses to recent climate change in high-mountain Asia. *Scientific Reports*, *7*, 13717. <https://doi.org/10.1038/s41598-017-14256-5>
- Scherler, D., Bookhagen, B., & Strecker, M. R. (2011). Spatially variable response of Himalayan glaciers to climate change affected by debris cover. *Nature Geoscience*, *4*, 156–159. <https://doi.org/10.1038/NGEO1068>
- Shean, D. E., Bhushan, S., Montesano, P., Rounce, D. R., Arendt, A., & Osmanoglu, B. (2020). A systematic, regional assessment of high mountain Asia glacier mass balance. *Frontiers in Earth Science*, *7*, 363. <https://doi.org/10.3389/feart.2019.00363>
- Shi, Y., & Liu, S. (2000). Estimation on the response of glaciers in China to the global warming in the 21st century. *Chinese Science Bulletin*, *45*(7), 668–672. <https://doi.org/10.1007/bf02886048>
- Shi, Y., Liu, S., Ye, B., Liu, C., & Wang, Z. (2008). *Concise glacier inventory of China*. Shanghai Popular Science Press.
- Sun, J., Yang, K., Guo, W., Wang, Y., He, J., & Lu, H. (2020). Why has the inner Tibetan Plateau become wetter since the mid-1990s? *Journal of Climate*, *33*(19), 8507–8522. <https://doi.org/10.1175/JCLI-D-19-0471.1>
- Sunako, S., Fujita, K., Sakai, A., & Kayastha, R. B. (2019). Mass balance of Trambau Glacier, Rolwaling region, Nepal Himalaya: In-situ observations, long-term reconstruction and mass-balance sensitivity. *Journal of Glaciology*, *65*(252), 605–616. <https://doi.org/10.1017/jog.2019.37>
- Thompson, L. G., Davis, M. E., Mosley-Thompson, E., Porter, S. E., Corrales, G. V., Shuman, C. A., & Tucker, C. J. (2021). The impacts of warming on rapidly retreating high-altitude, low-latitude glaciers and ice core-derived climate records. *Global and Planetary Change*, *203*, 103538. <https://doi.org/10.1016/j.gloplacha.2021.103538>
- Thompson, L. G., Yao, T., Davis, M. E., Mosley-Thompson, E., Wu, G., Porter, S. E., et al. (2018). Ice core records of climate variability on the Third Pole with emphasis on the Guliya ice cap, western Kunlun Mountains. *Quaternary Science Reviews*, *188*, 1–14. <https://doi.org/10.1016/j.quascirev.2018.03.003>
- Tian, L., Zong, J., Yao, T. Y., Ma, L. M., Pu, J. P., & Zhu, D. (2014). Direct measurement of glacier thinning on the southern Tibetan Plateau (Gurenhekou, Kangwure and Naimona'nyi glaciers). *Journal of Glaciology*, *60*(223), 879–888. <https://doi.org/10.3189/2014Jog14J022>
- Wang, Q., Yi, S., & Sun, W. (2021). Continuous estimates of glacier mass balance in High Mountain Asia based on ICESat-1, 2 and GRACE/GRACE follow-on data. *Geophysical Research Letters*, *48*(2), e2020GL090954. <https://doi.org/10.1029/2020GL090954>
- Wang, R., Liu, S., Shangguan, D., Radić, V., & Zhang, Y. (2019). Spatial heterogeneity in glacier mass-balance sensitivity across High Mountain Asia. *Water*, *11*, 776. <https://doi.org/10.3390/w11040776>
- Wang, Y., Hou, S., Huai, B., An, W., Pang, H., & Liu, Y. (2018). Glacier anomaly over the western Kunlun Mountains, Northwestern Tibetan Plateau, since the 1970s. *Journal of Glaciology*, *64*(246), 624–636. <https://doi.org/10.1017/jog.2018.53>
- WGMS. (2020). Global Glacier Change Bulletin No. 3 (2016–2017). In M. Zemp, S. U. Nussbaumer, I. Gärtner-Roer, M. Hoelzle, F. Paul, & W. Haeberli (Eds.), *Zürich: ICSU (WDS)/IUGG (IACS)/UNEP/UNESCO/WMO* (Vol. 3). World Glacier Monitoring Service. Retrieved from <https://10.5904/wgms-fog-2019-12>
- Wu, K., Liu, S., Jiang, Z., Xu, J., Wei, J., & Guo, W. (2018). Recent glacier mass balance and area changes in the Kangri Karpo Mountains from DEMs and glacier inventories. *The Cryosphere*, *12*(1), 103–121. <https://doi.org/10.5194/tc-12-103-2018>
- Xie, P., & Arkin, P. A. (1997). Global precipitation: A 17-year monthly analysis based on gauge observations, satellite estimates, and numerical model outputs. *Bulletin of the American Meteorological Society*, *78*, 2539–2558. [https://doi.org/10.1175/1520-0477\(1997\)078<2539:gpayma>2.0.co;2](https://doi.org/10.1175/1520-0477(1997)078<2539:gpayma>2.0.co;2)
- Yan, S., Liu, G., Wang, Y., Perski, Z., & Ruan, Z. (2015). Glacier surface motion pattern in the Eastern part of West Kunlun Shan estimation using pixel-tracking with PALSAR imagery. *Environmental Earth Sciences*, *74*(3), 1871–1881. <https://doi.org/10.1007/s12665-015-4645-7>
- Yang, W., Guo, X., Yao, T., Zhu, M., & Wang, Y. (2016). Recent accelerating mass loss of southeast Tibetan glaciers and the relationship with changes in macroscale atmospheric circulations. *Climate Dynamics*, *47*(3–4), 805–815. <https://doi.org/10.1007/s00382-015-2872-y>
- Yang, W., Yao, T., Guo, X., Zhu, M., Li, S., & Kattel, D. B. (2013). Mass balance of a maritime glacier on the southeast Tibetan Plateau and its climatic sensitivity. *Journal of Geophysical Research*, *118*(17), 9579–9594. <https://doi.org/10.1002/jgrd.50760>
- Yao, T., Masson-Delmotte, V., Gao, J., Yu, W., Yang, X., Risi, C., et al. (2013). A review of climatic controls on  $\delta^{18}\text{O}$  in precipitation over the Tibetan Plateau: Observations and simulations. *Reviews of Geophysics*, *51*(4), 525–548. <https://doi.org/10.1002/rog.20023>
- Yao, T., Thompson, L., Yang, W., Yu, W., Gao, Y., Guo, X., et al. (2012). Different glacier status with atmospheric circulations in Tibetan Plateau and surroundings. *Nature Climate Change*, *2*(9), 663–667. <https://doi.org/10.1038/nclimate1580>
- Yao, T., Thompson, L. G., Shi, Y., Qin, D., Jiao, K., Yang, Z., et al. (1997). Climate variation since the Last Interglaciation recorded in the Guliya ice core. *Science in China Series D: Earth Sciences*, *40*(6), 662–668. <https://doi.org/10.1007/BF02877697>
- Yao, T., Xue, Y., Chen, D., Chen, F., Thompson, L., Cui, P., et al. (2019). Recent third pole's rapid warming accompanies cryospheric melt and water cycle intensification and interactions between monsoon and environment: Multidisciplinary approach with observations, modeling, and analysis. *Bulletin of the American Meteorological Society*, *100*(3), 423–444. <https://doi.org/10.1175/Bams-D-17-0057.1>
- Yasuda, T., & Furuya, M. (2015). Dynamics of surge-type glaciers in West Kunlun Shan, northwestern Tibet. *Journal of Geophysical Research: Earth Surface*, *120*(11), 2393–2405. <https://doi.org/10.1002/2015JF003511>
- Yasui, S., & Watanabe, M. (2010). Forcing processes of the summertime circumpolar teleconnection pattern in a dry AGCM. *Journal of Climate*, *23*, 2093–2114. <https://doi.org/10.1175/2009JCLI3323.1>
- Ye, Q., Zong, J., Tian, L., Cogley, J. G., Song, C., & Guo, W. (2017). Glacier changes on the Tibetan Plateau derived from Landsat imagery: Mid-1970s–2000–13. *Journal of Glaciology*, *63*, 273–287. <https://doi.org/10.1017/jog.2016.137>
- Zhang, G., Chen, W., Li, G., Yang, W., Yi, S., & Luo, W. (2020). Lake water and glacier mass gains in the northwestern Tibetan Plateau observed from multi-sensor remote sensing data: Implication of an enhanced hydrological cycle. *Remote Sensing of Environment*, *237*, 111554. <https://doi.org/10.1016/j.rse.2019.111554>
- Zhang, H., Li, Z., & Zhou, P. (2021). Mass balance reconstruction for Shiyi Glacier in the Qilian Mountains, northeastern Tibetan Plateau, and its climatic drivers. *Climate Dynamics*, *56*(3), 969–984. <https://doi.org/10.1007/s00382-020-05514-w>
- Zhang, Y., Hirabayashi, Y., Liu, Q., & Liu, S. (2015). Glacier runoff and its impact in a highly glacierized catchment in the southeastern Tibetan Plateau: Past and future trends. *Journal of Glaciology*, *61*(228), 713–730. <https://doi.org/10.3189/2015Jog14J188>

- Zhao, H., Yao, T., & Xu, B. (2021). High-elevation climate changes recorded in Tibetan ice cores and their impact on glacier behavior. *Palaeogeography, Palaeoclimatology, Palaeoecology*, 576, 110506. <https://doi.org/10.1016/j.palaeo.2021.110506>
- Zhao, Q., Ye, B., He, X., Zhang, J., & Zhao, C. (2014). Bias correction of daily precipitation measured by Geonor T-200B precipitation gauge in Tanggula Mountain. *Plateau Meteorology*, 33(2), 452–459. [in Chinese]. <https://doi.org/10.7522/j.issn.1000-0534.2013.00013>
- Zhao, Y., Huang, A., Zhou, Y., Huang, D., Yang, Q., Ma, Y., et al. (2014). Impact of the middle and upper tropospheric cooling over central Asia on the summer rainfall in the Tarim Basin, China. *Journal of Climate*, 27(12), 4721–4732. <https://doi.org/10.1175/JCLI-D-13-00456.1>
- Zhou, Y., Li, Z., Li, J., Zhao, R., & Ding, X. (2018). Glacier mass balance in the Qinghai–Tibet Plateau and its surroundings from the mid-1970s to 2000 based on Hexagon KH-9 and SRTM DEMs. *Remote Sensing of Environment*, 210, 96–112. <https://doi.org/10.1016/j.rse.2018.03.020>
- Zhu, M., Thompson, L. G., Zhao, H., Yao, T., Yang, W., & Jin, S. (2021). Influence of atmospheric circulation on glacier mass balance in western Tibet: An analysis based on observations and modeling. *Journal of Climate*, 34(16), 6743–6755. <https://doi.org/10.1175/JCLI-D-20-0988.1>
- Zhu, M., Yang, W., Yao, T., Tian, L., Thompson, L. G., & Zhao, H. (2021). The influence of key climate variables on mass balance of Naimona'nyi Glacier on a north-facing slope in the western Himalayas. *Journal of Geophysical Research*, 126, e2020JD033956. <https://doi.org/10.1029/2020JD033956>
- Zhu, M., Yao, T., Xie, Y., Xu, B., Yang, W., & Yang, S. (2020). Mass balance of Muji Glacier, northeastern Pamir, and its controlling climate factors. *Journal of Hydrology*, 590, 125447. <https://doi.org/10.1016/j.jhydrol.2020.125447>
- Zhu, M., Yao, T., Yang, W., Xu, B., Wu, G., & Wang, X. (2018a). Differences in mass balance behavior for three glaciers from different climatic regions on the Tibetan Plateau. *Climate Dynamics*, 50(9–10), 3457–3484. <https://doi.org/10.1007/s00382-017-3817-4>
- Zhu, M., Yao, T., Yang, W., Xu, B., Wu, G., Wang, X., & Xie, Y. (2018b). Reconstruction of the mass balance of Muztag Ata No. 15 glacier, eastern Pamir, and its climatic drivers. *Journal of Glaciology*, 64(244), 259–274. <https://doi.org/10.1017/jog.2018.16>

## References From the Supporting Information

- Fujita, K., Thompson, L. G., Ageta, Y., Yasunari, T., Kajikawa, Y., Sakai, A., & Takeuchi, N. (2006). Thirty-year history of glacier melting in the Nepal Himalayas. *Journal of Geophysical Research*, 111(D3). <https://doi.org/10.1029/2005JD005894>
- Hanna, E., Huybrechts, P., Janssens, I., Cappelen, J., Steffen, K., & Stephens, A. (2005). Runoff and mass balance of the Greenland ice sheet: 1958–2003. *Journal of Geophysical Research*, 110(D13). <https://doi.org/10.1029/2004JD005641>
- Philippe, M., Tison, J.-L., Fjøsne, K., Hubbard, B., Kjær, H. A., Lenaerts, J. T. M., et al. (2016). Ice core evidence for a 20th century increase in surface mass balance in coastal Dronning Maud Land, East Antarctica. *The Cryosphere*, 10, 2501–2516. <https://doi.org/10.5194/tc-10-2501-2016>
- Purdie, H., Mackintosh, A., Lawson, W., Anderson, B., Morgenstern, U., Chinn, T., & Mayewski, P. (2011). Interannual variability in net accumulation on Tasman Glacier and its relationship with climate. *Global and Planetary Change*, 77(3–4), 142–152. <https://doi.org/10.1016/j.gloplacha.2011.04.004>